Comparative analysis reveals distinct actin-based motility mechanisms in divergent *Rickettsia* species

Meghan C. Bacher[1], Julie E. Choe, Jiawen Jiang[2], and Matthew D. Welch[1]

[1]Department of Molecular and Cell Biology, University of California, Berkeley, Berkeley, CA, USA; [2]Department of Plant and Microbial Biology, University of California, Berkeley, Berkeley, CA, USA

Correspondence:
Matthew D. Welch
Department of Molecular and Cell Biology
301 Weill Hall
University of California, Berkeley
Berkeley, CA 94720-3200
welch@berkeley.edu

Abstract

After invading host cells and accessing the cytoplasm, many *Rickettsia* species undergo actin-based motility driven by two bacterial proteins, RickA and Sca2. In the spotted fever group species *R. parkeri*, this motility occurs in temporally and mechanistically distinct phases. Early in infection, RickA drives motility by activating the host Arp2/3 complex to nucleate actin; later, Sca2 independently drives motility by directly nucleating and elongating actin via a formin-like mechanism. The distantly related and non-pathogenic species *R. bellii* also expresses RickA and Sca2 orthologs, but how each contributes to the mechanism and timing of motility remains unclear. *R. bellii* Sca2 differs substantially from *R. parkeri* Sca2 in primary sequence, and we found that the *R. bellii* protein nucleates and elongates actin using an unusual N-terminal actin monomer-binding domain yet does not processively associate with growing actin filaments like *R. parkeri* Sca2 or eukaryotic formins. Notably, actin-based motility in *R. bellii* occurs only later in infection and strongly correlates with a highly polarized localization of Sca2 at one bacterial pole. In contrast, *R. bellii* motility is independent of RickA localization and Arp2/3 complex function. Compared to *R. parkeri*, *R. bellii* moves more slowly and along less direct paths, with actin tails exhibiting a distinct organization that reflects differences in Sca2 mechanism and localization. Together, these findings demonstrate substantial evolutionary flexibility in actin-based motility mechanisms within the *Rickettsia* genus and suggest similar adaptability among other intracellular microbes.

Introduction

Intracellular bacteria have evolved numerous ways to co-opt the host cell actin cytoskeleton for processes including invasion, innate immune avoidance, and cell-cell spread (Colonne *et al.*, 2016; Lamason and Welch, 2017; Stradal and Schelhaas, 2018). Actin-based motility is one mechanism through which actin contributes to cell-cell spread. This process uses the force derived from the nucleation and elongation of actin filaments at the bacterial surface to drive movement through the host cell cytoplasm, resulting in the assembly of actin comet tails (Gouin *et al.*, 2005; Lamason and Welch, 2017). The ensuing motility positions bacteria near the host cell plasma membrane to enable them to enter membrane protrusions that can be engulfed into neighboring cells (Lamason and Welch, 2017).

The mechanism of actin-based motility has been studied for a variety of pathogens including *Rickettsia* species (Lamason and Welch, 2017; Alqassim, 2022). *Rickettsia* are Gram-negative obligate intracellular alphaproteobacteria that typically reside in arthropods such as ticks, fleas, and mites (Guillotte *et al.*, 2021). The *Rickettsia* genus is divided into 5 distinct groups clustered by molecular phylogenomics and disease features (Karkouri *et al.*, 2022; Rymaszewska and Piotrowski, 2024). These groups include the spotted fever groups (SFG I/II) and typhus group (TG), which contain pathogens that cause spotted fever and typhus in humans. They also include the canadensis group (CG) and bellii group (BG), which contain species considered to be non-pathogenic tick endosymbionts. Actin-based motility has been observed for species within most of the groups including the SFG I species, *R. parkeri*, and BG species, *R. bellii* (Teysseire *et al.*, 1992; Heinzen *et al.*, 1993; Gouin *et al.*, 1999; Van Kirk *et al.*, 2000; Haglund *et al.*, 2010; Pan *et al.*, 2022).

Rickettsia species are distinctive amongst microbes that undergo actin-based motility in that their genomes often encode two different motility effectors, RickA and Sca2 (Blanc *et al.*, 2005; Haglund *et al.*, 2010; Kleba *et al.*, 2010; Reed *et al.*, 2014; Gillespie *et al.*, 2015; Narra *et al.*, 2020). Studies with the SFG I species, *R. parkeri*, harboring transposon mutants in *rickA* or *sca2* demonstrated that RickA and Sca2 function independently to drive two temporal phases of motility (Reed *et al.*, 2014). RickA-motility occurs at early time points of infection (< 2 h post-infection (hpi)), is slower, and proceeds in meandering trajectories, resulting in actin tails that are short and curved (Jeng *et al.*, 2004; Reed *et al.*, 2014). Sca2-motility occurs later (> 5 hpi), is faster, and proceeds via linear trajectories, resulting in actin tails that are long and straight (Reed *et al.*, 2014). Disruptions in *rickA* and *sca2* lead to the formation of smaller plaques during infection, indicating both RickA-motility and Sca2-motility contribute to cell-cell spread (Kleba *et al.*, 2010; Reed *et al.*, 2014; Tran *et al.*, 2025). However, the modes of spread differ in key parameters. RickA-spread results from the formation of longer and more dynamic plasma membrane protrusions, whereas Sca2-spread results from the formation of shorter and less dynamic protrusions (Lamason *et al.*, 2016; Tran *et al.*, 2025). In a mouse model of infection, RickA is important for eschar formation in the skin, whereas Sca2 is important for dissemination to internal organs (Burke *et al.*, 2021; Tran *et al.*, 2025).

In addition to differences in their roles in cell-cell spread and pathogenicity, RickA and Sca2 from SFG I species nucleate actin filaments through different biochemical mechanisms. RickA is secreted by bacteria through an unknown mechanism and acts as a nucleation-promoting factor (NPF) that activates the host Arp2/3 complex through conserved C-terminal WH2, central, and acidic (WCA) motifs (Gouin *et al.*, 2004; Jeng *et al.*, 2004). Activated Arp2/3 complex nucleates a new actin filament from the side of an existing filament in a Y-branched configuration (Gautreau *et al.*, 2022). Sca2 is a type V secretion system (T5SS) or autotransporter protein, a family of proteins that consists of an N-terminal signal sequence that enables passage through

the bacterial inner membrane, a C-terminal translocation domain consisting of a β-barrel structure that embeds in the outer membrane, and a central passenger domain that threads through the translocation domain and is displayed on the bacterial surface (Fan *et al.*, 2016). The Sca2 passenger domain from SFG I species nucleates and processively elongates actin filaments in a profilin-dependent manner, similar to eukaryotic formin proteins (Haglund *et al.*, 2010; Madasu *et al.*, 2013; Alqassim *et al.*, 2019). Within the passenger domain, the middle domain binds to an actin monomer, and the N-terminal domain (NTD) folds into a ring structure resulting in a formin-like core that cooperatively binds two actin monomers with high affinity in conjunction with the C-terminal repeat domain (CRD) (Alqassim *et al.*, 2019; Carman *et al.*, 2023). Interestingly, the passenger domain of Sca2 from the divergent BG species, *R. bellii*, differs dramatically in sequence from SFG I Sca2 (Haglund *et al.*, 2010). However, we do not yet know whether and how sequence or regulatory differences in RickA or Sca2 contribute to differences in the mechanism and properties of actin-based motility in diverse *Rickettsia* species.

To better understand the functions of RickA and Sca2 in divergent *Rickettsia* species, we compared the actin nucleation mechanisms, protein localization, and motility characteristics between the non-pathogenic tick endosymbiont *R. bellii* and the well-studied pathogenic SFG I species *R. parkeri*. We found that the Arp2/3-dependent actin nucleation mechanism of RickA is conserved. However, *R. bellii* Sca2 nucleates and elongates actin filaments by a mechanism that differs from the formin-like mechanism of SFG I Sca2. Unexpectedly, in infected cells, *R. bellii* motility did not occur early in infection, was functionally independent of RickA and the Arp2/3 complex, and was tightly correlated with polar Sca2 localization. Differences in Sca2 mechanism and localization between *R. bellii* and *R. parkeri* also correlated with differences in actin tail organization and actin-based motility. Together, these data indicate that there is considerable evolutionary flexibility in actin-based motility proteins and mechanisms within the *Rickettsia* genus.

Results

RickA is conserved while Sca2 has diverged in *R. bellii.*

To better understand how RickA and Sca2 have diverged across *Rickettsia* species, we aligned the RickA and Sca2 protein sequences from representative *Rickettsia* species from the SFG I/II, TG (Sca2 only) and BG groups, including *R. parkeri* strain Portsmouth and *R. bellii* strain RML 369-C. For RickA, the overall organization of sequence motifs is conserved (Figure 1A). Alignment of RickA protein sequences (Figure S1A) showed that the C-terminal WCA region exhibits 27% sequence identity and 56% similarity overall. SFG I and BG species contain a single WH2 motif, whereas SFG II species contain two WH2 motifs (Figure 1A and S1A). This high degree of conservation suggests that the biochemical function and activities of RickA are conserved between species.

In contrast, Sca2 proteins from divergent species differ considerably in the organization of sequence motifs in the passenger domain (Figure 1B). In comparison with Sca2 from the SFG I species *R. parkeri* (1823 amino acids), Sca2 from *R. bellii* is half as long (909 amino acids) and lacks the N-terminal repeats within the NTD and CRD domains that were previously shown to form a partially occluded formin-like core (Figure 1B, S1B) (Haglund *et al.*, 2010; Madasu *et al.*, 2013; Alqassim *et al.*, 2019; Carman *et al.*, 2023). The passenger domains of Sca2 only exhibit 11% percent identity and 33% similarity (Figure S1B). Using a combination of AlphaFold 3 and InterPro protein domain predictions (Abramson *et al.*, 2024; Blum *et al.*, 2024), we annotated the passenger domain of *R. bellii* Sca2 as having a signal sequence (S), a poly-proline region

(P), putative G-actin binding domain (G) previously annotated as a WH2 motif (Haglund *et al.*, 2010), and a C-terminal domain (CTD) (Figure 1B, S1B). As described for Sca2 from the SFG I species *R. conorii*, the previously annotated WH2 motifs (Haglund *et al.*, 2010) in *R. bellii* Sca2 are predicted to have different secondary structures than canonical WH2 domains (Ducka *et al.*, 2010; Dominguez, 2016). Nevertheless, AlphaFold 3 structure predictions suggested that an α-helix within the previously annotated WH2 motif of *R. bellii* Sca2 may bind to an actin monomer at the barbed end (pLDDT > 70, Figure S2). This updated analysis confirms that the passenger domain of the Sca2 protein differs substantially between *R. bellii* and the SFG I species *R. parkeri*, suggesting potential differences in biochemical activities and mechanisms of action.

We also sought to confirm that *R. bellii* expresses RickA and Sca2 orthologues, as does *R. parkeri* (Haglund *et al.*, 2010; Reed *et al.*, 2014). Both proteins were detected in *R. bellii* bacterial lysates by immunoblotting with anti-RickA or anti-Sca2 antibodies (Figure S3). Thus, *R. bellii* expresses both actin-based motility effector proteins.

R. bellii RickA activates the host Arp2/3 complex *in vitro*.

RickA proteins from the SFG I species, *R. rickettsii* (Jeng *et al.*, 2004) and *R. conorii* (Gouin *et al.*, 2004), were previously shown to function as NPFs and activate the host Arp2/3 complex. To test whether RickA from *R. bellii* also possesses NPF activity, we expressed and purified GST-tagged RickA (GST-RickA) and performed pyrene actin polymerization assays (Figure S4). Purified GST-RickA or Arp2/3 complex individually showed no enhancement in actin polymerization activity compared to actin alone. However, when combined, GST-RickA activated the Arp2/3 complex in a concentration-dependent manner. These data confirm that *R. bellii* RickA has NPF activity.

R. bellii Sca2 nucleates and elongates actin filaments *in vitro*.

Our comparisons of Sca2 proteins from *R. parkeri* and *R. bellii* suggested that the biochemical activity of *R. bellii* Sca2 may differ considerably from that of *R. parkeri* Sca2, which nucleates actin assembly and caps actin filaments in the absence of profilin (Haglund *et al.*, 2010; Madasu *et al.*, 2013). To determine whether *R. bellii* Sca2 nucleates actin assembly, we expressed and purified the MBP-tagged passenger domain of Sca2 (MBP-Sca2; excluding the signal sequence and autotransporter domains) and performed pyrene actin polymerization assays. Purified MBP-Sca2 alone nucleated actin assembly in a concentration-dependent manner (Figure 2A). Cleavage of the MBP tag did not significantly impact actin nucleation activity (Figure S5A). For comparison, *R. parkeri* GST-Sca2 alone also nucleated actin filament assembly, but fluorescence plateaued at a lower value due to its barbed end capping activity in the absence of profilin (Haglund *et al.*, 2010) (Figure 2A). Thus, *R. bellii* Sca2 nucleates actin assembly without capping the barbed end of actin filaments.

R. parkeri Sca2 processively associates with barbed ends and enables filament elongation in the presence of profilin (Haglund *et al.*, 2010; Madasu *et al.*, 2013), like eukaryotic formins (Breitsprecher and Goode, 2013; Valencia and Quinlan, 2021). For comparison, we sought to assess whether *R. bellii* Sca2 stably associates with actin filaments and/or affects the rate of filament elongation using total internal reflection fluorescence (TIRF) microscopy. We fluorescently labeled the C-terminus of *R. bellii* Sca2 with Alexa Fluor 647 (AF647) and cleaved the MBP-tag to create Sca2-AF647. Sca2-AF647 and MBP-Sca2 activity were similar in pyrene actin assays (Figure S5). Polymerization of 1 μM actin was initiated in the absence or presence of Sca2-AF647 and the growth of actin filaments was visualized with TIRF microscopy. We did not observe stable association of Sca2 puncta with polymerizing actin filaments over a range of

Sca2-AF647 concentrations (Movie S1). However, transient interactions between Sca2-AF647 puncta and the sides or ends of growing filaments were sometimes spotted. The rate of barbed end growth was modestly (~1.25-fold), but statistically significantly, increased in the presence of Sca2-AF647 when compared with actin alone (Figure 2B and C). The addition of 3 μM profilin to Sca2-AF647 diminished the elongation rate to that of actin alone (Figure 2B and C). Together, these data show that *R. bellii* Sca2 nucleates actin and modestly enhances actin elongation independent of profilin and without detectable processive association with filament ends.

An N-terminal actin-binding sequence in *R. bellii* Sca2 is necessary for actin nucleation activity.

To determine which domains of *R. bellii* Sca2 contribute to its actin nucleation activity, we expressed and purified a series of truncation mutants including: MBP-ΔpolyPSca2 (missing the poly-proline region), MBP-NTDSca2 (missing the C-terminus), or MBP-Sca2CTD (missing the N-terminus) (Figure 3A). We performed pyrene actin assembly assays with 70 nM of each of these proteins and calculated the time to reach half maximum fluorescence ($t_{1/2\ max}$) values to compare their actin nucleation activities. MBP-ΔpolyPSca2 exhibited actin nucleation activity that was not distinguishable from full-length Sca2 (Figure 3B). The activity of MBP-NTDSca2 was significantly reduced in comparison with full-length Sca2, but polymerization was enhanced relative to actin alone (Figure 3B). In comparison, MBP-Sca2CTD did not exhibit actin nucleation activity (Figure 3B). Together, these data suggest that sequences in the NTD of *R. bellii* Sca2 between the poly-proline sequence and CTD are necessary, but not sufficient for full nucleation activity.

To test the importance of the predicted G-actin binding motif in the NTD, we expressed and purified a version of Sca2 where L101 and K102 were both substituted with alanine (MBP-Sca2-L101A/K102A). These amino acid substitutions substantially reduced the confidence of AlphaFold 3 predictions for actin-binding (pLDDT < 50, Figure S2). The purified MBP-Sca2-L101A/K102A protein did not show actin nucleation activity with a $t_{1/2\ max}$ value comparable to actin alone (Figure 3B). Furthermore, MBP-Sca2-L101A/K102A showed no nucleation activity above background levels at concentrations ranging from 10 – 250 nM in contrast to the clear nucleation activity of MBP-Sca2 over the same concentration range (Figure 3C). These data demonstrate that the proposed G-actin binding domain is necessary for the actin nucleation activity of *R. bellii* Sca2.

***R. bellii* has a single phase of actin-based motility in mammalian cell lines**

Although both *R. bellii* RickA and Sca2 are biochemically active, their roles in *R. bellii* actin-based motility have not been determined. Our prior work with *R. parkeri* showed that this species exhibits two phases of motility; an early (<2 hpi) phase driven by RickA and a late phase (>5 hpi) driven by Sca2 (Reed *et al.*, 2014). To determine if *R. bellii* also exhibits this same biphasic motility pattern, we infected human A549 epithelial or HMEC-1 endothelial cell lines with either *R. parkeri* or *R. bellii* and quantified the frequency at which bacteria assemble actin tails between 15 min post-infection (mpi) and 24 hpi as a measure of the frequency of actin-based motility. Actin tails were observed throughout the 24 h time course in *R. parkeri*-infected cells, with two peaks in actin tail frequency corresponding to the early RickA-motility (15 - 30 mpi, A = 5.6 – 6.0%, H = 8.3 – 9.5%) and late Sca2-motility (16 hpi - 24 hpi, A = 9.6 – 13.8%, H = 21.6 – 28.5%) phases (Figure 4A and B). In contrast, *R. bellii* actin tails were extremely rare prior to 8 hpi in both cell lines. The frequency of *R. bellii* actin tails increased from 8 hpi through 24 hpi (A = 9.5 – 42.4%, H = 7.0 – 27.1%). These results suggest that *R. bellii* exhibits only a single phase of actin-based motility in infected mammalian cell lines.

No role was observed for *R. bellii* RickA and host Arp2/3 complex in actin-based motility.

To investigate a possible role for RickA in *R. bellii* actin-based motility at 8 h and 24 h post-infection, we first localized surface-associated RickA and actin by fluorescence microscopy in infected A549 cells. Although actin tails were clearly observed at both time points, we did not observe RickA on the bacterial surface (Figure 5A and B). Next, to localize intra-bacterial RickA, we permeabilized bacteria with lysozyme. A subset of bacteria showed evidence of internal RickA staining (Total RickA; Figure 5A and B), consistent with our immunoblotting data showing RickA is expressed by *R. bellii* (Figure S3). These data suggest that RickA is not localized to the bacterial surface under the conditions tested and therefore its surface localization is not correlated with actin-based motility. Immunostaining for specific Arp2/3 complex components, anti-p34 and anti-ArpC3, also did not show surface localization to bacteria with actin tails (data not shown).

To examine the functional importance of RickA, we leveraged the dependency of RickA-motility on the host Arp2/3 complex and the availability of small-molecule Arp2/3 complex inhibitors CK-666 and CK-869, as well as inactive control compound CK-689 (Nolen *et al.*, 2009; Cao *et al.*, 2024). As a positive control, we evaluated the effect of 1 h treatment with these compounds on *L. monocytogenes* actin-based motility in infected A549 cells, a process that is known to depend on the Arp2/3 complex (Welch *et al.*, 1997). As expected, *L. monocytogenes* actin tail frequency was significantly reduced in the presence of CK-666 or CK-869 compared to the inactive control drug (Figure 5C). In contrast, for *R. bellii*-infected A549 cells at either 8 hpi or 24 hpi, actin tail frequencies were not significantly different following 1 h treatment with the Arp2/3 complex inhibitors CK-666 or CK-869 versus the inactive control compound (Figure 5C). Together, these data suggest that, while RickA is biochemically active, RickA- and Arp2/3 complex-dependent actin-based motility was not observed in *R. bellii*-infected human cell lines.

Sca2 surface localization is correlated with *R. bellii* actin-based motility.

We next investigated a role for Sca2 in *R. bellii* actin-based motility at 8 h and 24 h post-infection by localizing surface-associated Sca2 and actin by confocal microscopy in infected A549 cells. Sca2 exhibited a focused localization at the poles of ~40% of the bacteria at 8 hpi and ~80% of bacteria at 24 hpi (Figure 6A and B). A majority of bacteria with polar Sca2 foci had an associated actin tail. Moreover, for all bacteria with an actin tail in this data set, the actin tail emerged from the bacterial pole with Sca2 (Figure 6A). Therefore, Sca2 localization to the surface of *R. bellii* is tightly correlated with actin-based motility.

Sca2 localization and actin tail architecture differ between *Rickettsia* species.

Sca2 localization to a discrete focus at the *R. bellii* pole seemed distinct compared with its previously reported localization in a more cup-shaped pattern at the pole of *R. parkeri* (Haglund *et al.*, 2010; Reed *et al.*, 2014). To directly compare differences in Sca2 localization patterns on the surface of *R. parkeri* versus *R. bellii*, we imaged *Rickettsia*-infected A549 cells at 24 hpi using a super-resolution lattice structured illumination microscope (LSIM) and further deconvolved the images to reduce image distortion. *R. parkeri* Sca2 tended to coat the bacterial pole associated with an actin tail or even the entire bacterium, while *R. bellii* Sca2 localized to the bacterial pole as a distinct punctum (Figure 7A). We further quantified the surface area and sphericity of the Sca2 signal, along with the overlapped volume between the Sca2 and the bacterial signals. Sca2 occupied a larger surface area (Figure 7B) and exhibited a greater overlap with the bacterium (Figure 7C) for *R. parkeri* compared with *R. bellii*. Sca2 localization

was significantly more spherical for *R. bellii* than *R. parkeri* (Figure 7D). Therefore, Sca2 exhibits a more extreme polar localization on *R. bellii* compared to *R. parkeri*.

Corresponding with differences in Sca2 localization, the architecture of the actin tails in the LSIM images was distinct for *R. parkeri* and *R. bellii* at 24 hpi, when Sca2-motility is predominant for both species. *R. parkeri* actin tails typically had two bands of actin emanating from the sides of the bacterial pole (Figure 7A and E), whereas *R. bellii* actin tails had a single band of actin centered on the Sca2 punctum (Figure 7A and E). To quantify the spatial organization of actin tails we took a line intensity scan of actin fluorescence perpendicular to the long axis of the actin tail (0.5 μm from the bacterial pole). Actin tails showed two distinct intensity peaks spaced 0.30 ± 0.09 μm apart, whereas *R. bellii* actin tails showed a single intensity peak (Figure 7F). The correlation between Sca2 localization and actin intensity profiles suggest that differences in Sca2 localization may impact differences actin tail organization between *Rickettsia* species.

Differences in Sca2 mechanism and localization as well as host cell type correlate with differences in actin-based motility.

We lastly looked at the functional consequences of differences in Sca2 biochemical mechanism and localization on actin-based motility parameters. We carried out live-cell imaging of *R. parkeri*- or *R. bellii*-infected A549 or HMEC-1 cells stably expressing F-tractin-TagRFPT (Johnson and Schell, 2009) at 24 hpi for 5 min and analyzed the actin-based motility speed and efficiency for each *Rickettsia* species and host cell combination. *R. parkeri* motility was significantly faster in A549 cells (mean 21 ± 5 μm/s) compared with HMEC-1 cells (mean 11 ± 4 μm/s). *R. bellii* moved more slowly than *R. parkeri* and with indistinguishable rates in A549 (mean 8 ± 3 μm/s) versus HMEC-1 cells (mean 9 ± 3 μm/s) (Figure 8A, Movie S2). We also measured the motility efficiency (defined as the straight-line distance between the starting and stopping points (Δd) in a 1 min interval, divided by the total distance traveled (D) during the interval, or Δd/D). *R. parkeri* motility efficiency was higher in both host cell lines (A549 mean 0.8 ± 0.2; HMEC-1 mean 0.8 ± 0.2) than for *R. bellii* (A = 0.6 ± 0.3, H = 0.7 ± 0.2) (Figure 8B, Movie S3). Traces of representative bacterial motility paths revealed more curved paths for *R. bellii* than for *R. parkeri*, particularly in A549 cells (Figure 8C). Thus, differences in Sca2 mechanism and localization correlate with slower *R. bellii* speed and lower motility efficiency compared with *R. parkeri*.

Notably, the organization of *R. bellii* actin tails was dramatically different in A549 versus HMEC-1 cells. In A549 cells, *R. bellii* actin tails were consolidated, consisting of a single bundle of actin filaments (Figure 7A and 8D). However, in HMEC-1 cells, *R. bellii* actin tails were disorganized, consisting of multiple bundles of actin filaments splaying from the bacterial pole (Figure 8D). As noted above, *R. parkeri* actin tails appeared similar in organization in the different cell types (Figure 7A and 8D). Thus, differences in Sca2 mechanism and localization also correlate with cell type-specific differences in *R. bellii* actin-tail organization.

Discussion

Our results provide insight into how the mechanisms and functions of actin-based motility effectors have evolved within the *Rickettsia* genus. We find that RickA has maintained its ability to activate the host Arp2/3 complex to nucleate actin filaments, but its function in actin-based motility is not conserved between groups of *Rickettsia* species. Sca2, on the other hand, contributes to actin-based motility in divergent *Rickettsia* species, but its sequence and mechanism differs substantially between species. Divergent Sca2 nucleation mechanisms

coupled with different localization patterns on the bacterial surface contribute to differences in actin organization and motility. Our data indicate there is considerable evolutionary plasticity in actin-based motility proteins and mechanisms within the *Rickettsia* genus.

In *R. parkeri*, RickA-motility was previously shown to occur early after infection of a host cell and to function in cell-cell spread (Reed *et al.*, 2014; Tran *et al.*, 2025). Although we now report that *R. bellii* bacteria express a RickA protein that possesses Arp2/3-dependent actin nucleation activity, we found no evidence for RickA localization to the surface of *R. bellii* and RickA or Arp2/3 complex function in *R. bellii* actin-based motility. The conservation of RickA in divergent species (Lehman *et al.*, 2024), despite the genus undergoing reductive genome evolution (Blanc *et al.*, 2007), suggests that RickA performs an important function. One explanation for our observations is that the function or regulation of RickA is host-dependent. SFG I species such as *R. parkeri* may have adapted to use RickA-motility in mammalian cells, whereas the tick endosymbiont *R. bellii* may only use RickA in tick cells. In support of this possibility, an *R. parkeri rickA* transposon mutant, but not a *sca2* mutant, showed reduced spread in ISE6 tick cells (Harris *et al.*, 2018). This further suggests potential differences in the regulation of RickA secretion between mammalian and tick hosts, and possible functions for RickA outside of actin-based motility.

As a result of the divergent Sca2 passenger domains, we report that the actin nucleation mechanism of Sca2 from *R. bellii* differs considerably from Sca2 from SFG I species *R. parkeri* and *R. conorii*. SFG I Sca2 nucleates actin, caps filaments in the absence of profilin, enables elongation in the presence of profilin, and processively associates with growing barbed ends, similar to eukaryotic formins (Haglund *et al.*, 2010; Madasu *et al.*, 2013; Alqassim *et al.*, 2019; Carman *et al.*, 2023). In contrast, we report that *R. bellii* nucleates and modestly enhances elongation in the absence of profilin and does not cap or stably associate with filament barbed ends, characteristics that differ from eukaryotic formins. The sequence and biochemical properties of *R. belliii* Sca2 also differ from other known host or microbial nucleators. We only identified a single actin monomer-binding domain in *R. bellii* Sca2 predicted to bind the barbed end of actin monomers and were unable to observe stable localization to either end of actin filaments. These properties differ from tandem WH2 nucleators, such as VopL/VopF (Vizcarra and Quinlan, 2017), which typically have 3-4 WH2 domains spaced by linkers and have been shown to dimerize for efficient actin nucleation at either the barbed or pointed end of an actin filament (Dominguez, 2016). *R. bellii* Sca2 also lacks key characteristics of host ENA/VASP nucleators, such as the ability to multimerize (Faix and Rottner, 2022). Based on our current understanding, *R. bellii* Sca2 therefore exhibits a distinctive mechanism of actin nucleation.

Our comparison of Sca2 localization in *R. parkeri* and *R. bellii* also reveals clear differences, with Sca2 in *R. bellii* exhibiting a more extreme polar distribution. Differences in localization may be a result of difference in protein secretion or processing. The *Shigella* actin-based motility effector IcsA is also a T5SS protein that is secreted at the bacterial pole and can diffuse across the surface, where it is cleaved by a protease (Shere *et al.*, 1997; Steinhauer *et al.*, 1999). When polar secretion is rapid, slower cleavage across the entire bacterial surface acts as a pruning mechanism to keep IcsA restricted to the bacterial pole (Shere *et al.*, 1997; Steinhauer *et al.*, 1999). Sca2 is also cleaved in *R. parkeri* (Haglund *et al.*, 2010; Reed *et al.*, 2014) and *R. bellii* (this study). Variations in location/rates of autotransporter secretion and protease activity may explain why Sca2 covers more of the bacterial surface of *R. parkeri* compared with *R. belli*.

At time points when Sca2 is the predominant motility effector for both *R. parkeri* and *R. bellii*, we observed clear differences in actin filament organization and actin-based motility. *R. parkeri* actin tails are organized into two discrete bundles that emerge from the sides of the bacterial

pole (Van Kirk *et al.*, 2000; Haglund *et al.*, 2010), and bacteria move more quickly and in straighter trajectories. *R. bellii* actin tails are organized into a single bundle, and bacteria move more slowly and in more meandering trajectories. Variations in motility likely derive from differences in Sca2 mechanisms of action and localization patterns. Differences in Sca2 biochemical activity may affect rates of actin elongation and/or filament capping at the bacterial surface. The fuller coverage of *R. parkeri* Sca2 on the bacterial surface and the resulting actin density that brackets the bacterial pole may steer the bacteria in straighter trajectories. In contrast, the extreme polar distribution of *R. bellii* Sca2 and the reduced actin density may contribute to more meandering motility and a smaller number of elongating actin filaments generating propulsive force. We also observed host cell type-specific differences, with disorganized *R. bellii* actin tails consisting of multiple splayed filament bundles in human endothelial cells. This actin tail architecture is reminiscent of the splayed *R. parkeri* actin tails observed in infected cells depleted of the actin-bundling protein fimbrin by siRNA (Serio *et al.*, 2010). *R. parkeri* bacteria, which naturally target human endothelial cells during infection (Scott *et al.*, 2022), retained a more consolidated actin tail phenotype in the endothelial cell line. Thus, differences in Sca2 localization, along with differences in the abundance and recruitment of host actin-bundling proteins or other actin associated proteins, likely play an important role in defining actin tail organization and bacterial movement parameters.

Together, our results provide insight into the evolution of actin-based motility mechanisms in microbial pathogens. While divergent species throughout the *Rickettsia* genus maintain the ability to undergo actin-based motility, the utilization of the two motility effectors RickA and Sca2, and the biochemical mechanisms of Sca2-mediated actin polymerization, have diverged. This evolution likely reflects changes in both motility effector sequences and regulation. Because of the diversity of *Rickettsia* genus, these bacteria provide a unique platform to unravel how actin-based motility evolved and contributes to pathogenicity or colonization. Future studies of how actin-based motility is affected by motility effector expression and localization, actin ultrastructure and organization, and the host cell environment, will provide powerful insights into both pathogen infection and host cell biology.

Materials and methods

Mammalian cell culture and cell line generation

Vero (CCL-81), HEK293T (CRL-3216), A549 (CRM-CCL-185), and HMEC-1 (CRL-3243) cells were sourced from the University of California, Berkeley, tissue culture facility. Vero cells were grown in DMEM containing 4.5 g/L D-glucose, 4 mM L-glutamine (Gibco, 11965118) and 2% fetal bovine serum (Gemini Bio-products, 100-500). HEK293T and A549 cells were grown in DMEM containing 4.5 g/L D-glucose, 4 mM L-glutamine (Gibco, 11965118), and 10% fetal bovine serum (ATLAS Biologics, FP-0500-A). HMEC-1 cells were grown in MCDB 131 (Sigma, M8537) containing 10 mM L-glutamine (Sigma, M8537-1L), 14 mM sodium bicarbonate, 10% fetal bovine serum (Hyclone, SH30071.03), 10 ng/ml EGF (BD Biosciences, 3540001), and 1 µg/ml hydrocortisone (Sigma, H0888). All cells were grown at 37˚C in 5% CO_2.

A549 or HMEC-1 cells expressing F-tractin-TagRFPT were generated through retroviral transduction with SC1205 as previously described (Lamason *et al.*, 2016). SC1205 (F-tractin-TagRFPT-pIPFCW2) was generated by subcloning the genes encoding F-tractin (flanked by NheI and XhoI restriction sites) (Johnson and Schell, 2009) and TagRFPT (flanked by XhoI and EcoRI restriction sites) (Shaner *et al.*, 2008) into NheI- and EcoRI-digested pIRES-puro (IP)-FCW2. Transduced cells were selected with 1 µg/mL puromycin (Sigma, P8833) and sorted

using the Aria Fusion Cell Sorter in the UC Berkeley Flow Cytometry Facility to select for cells that fell in the top 30% of brightness for RFP fluorescence.

Bacterial propagation and strain construction

R. parkeri strain Portsmouth was obtained from Chris Paddock at the Centers for Disease Control and prevention. *R. bellii* strain RML 369-C was obtained from Ted Hackstadt at the NIH/NIAID Rocky Mountain Laboratories. For propagation, *Rickettsia* bacteria were allowed to infect 5 confluent T175 flasks of Vero cells for 4-7 d at 33˚C until cells rounded and started to dissociate from the monolayer. Infected cells were scraped from the bottom of the flask into the growth media, pelleted, resuspended in 10 ml of K36 buffer (50 mM KH_2PO_4, 50 mM K_2HPO_4, pH 7.0, 100 mM KCl, 15 mM NaCl). Bacteria were released on ice from Vero cells by Dounce homogenization (50 strokes). Bacteria were isolated by centrifugation in a solution of 30% RenoCal-76 (Bracco Diagnostics, 04H208) in K36 buffer using a SW-32 Ti rotor (Beckman/Coulter) at 18,500 rpm for 30 min at 4˚C. The bacterial pellet was resuspended in 2 mL brain heart infusion (BHI) media (BD Difco, DF0418-17-7) and aliquoted before freezing at -80˚C.

Bacterial titers were determined by serially diluting the bacterial stock and performing a plaque assay in Vero cells. Briefly, serial dilutions in Vero cell media were used to infect a 6-well plate of Vero cells by centrifugation at 300 x g for 5 min at room temperature and overnight incubation at 33˚C. Cells were then overlaid in DMEM with 10% FBS (Gemini Bio-products, 100-500) and 0.5% (w/v) agarose (Sigma A9539). Once plaques appeared (5-7 d post-infection) cells were overlaid with a mixture of 1x PBS (Gibco, 10010072), 0.5% agarose, and 2.5% (v/v) neutral red (Sigma, N6264). Plaques were quantified the next day and used to calculate the plaque forming units (PFU) per mL.

Fluorescent *R. parkeri* or *R. bellii* expressing pRAM18dRGA (Burkhardt *et al.*, 2011) or pRAM18dR-2xCoTagBFP (Figueroa-Cuilan *et al.*, 2023) were generated by infecting a T75 flask of Vero cells with bacteria and incubating at 33˚C. Infected Vero cells were scraped up, resuspended in K36 buffer, and then broken open with 1 mm beads by two 30 s rounds of vortexing and resting on ice. Cell debris was pelleted, and the supernatant was washed 3x with 250 mM sucrose (ThermoFisher, S5). Washed bacteria were resuspended in 100 µL BHI and incubated on ice for 20 min with 10 µg of the plasmid. Bacteria were then electroporated in a 0.2 cm cuvette at 2.5 kV, 200 Ω, 25 µF. Electroporated bacteria were resuspended in 1.2 mL BHI and aliquoted onto Vero cells in 6-well plate (200 uL per well). The plate was centrifuged at 300 x g for 5 min at room temperature, and then incubated at 33˚C. The next day, 500 ng/mL rifampicin (Sigma, R3501; resuspended to 1 mg/mL in methanol and filter sterilized) was added to each well of infected Vero cells. After clear signs of infection were observed, *Rickettsia* were harvested by adding cold sterile water to each well for 2 min to break bacteria out of Vero cells. An equal amount of 2x BHI was added to each well and bacteria were frozen at -80˚C. After visually confirming fluorescent protein expression, bacteria were propagated as described above.

L. monocytogenes strain 10403S::dasherGFP was obtained from Daniel A. Portnoy at the University of California, Berkeley. *L monocytogenes* was streaked from frozen stocks onto BHI agar plates with 200 µg/mL spectinomycin and grown overnight at 37˚C. For infections, single colonies were used to seed overnight cultures in BHI with 200 µg/mL spectinomycin and were grown at 30˚C at a slant with no shaking.

Generating plasmids for protein expression

To generate plasmids pET-GST-RickA and pET-MBP-RickA to express *R. bellii* RickA tagged with glutathione-S transferase (GST) or maltose binding protein (MBP), the *R. bellii rickA* gene was amplified from boiled bacteria by PCR (primers: 5'-CTGTACTTCCAATCCAATGCAAAGATAACTGAGCTT- 3' and 5'-CCGTTATCCACTTCCAATCTACCTTTGTTGAGATTGTT-3'). To generate the plasmid pET-MBP-Sca2 to express *R. bellii* Sca2 tagged with MBP, the sequence encoding the Sca2 passenger domain (aa 43-630) excluding the secretion signal sequence and autotransporter domain was amplified from plasmid DNA by touchdown PCR (Korbie and Mattick, 2008) (primers: 5'-ACCTGTACTTCCAATCCAATGCACCACCTCCACCACCC_3' and 5'-ATCCGTTATCCACTTCCAATTCATTCATCACCACCAGTAATCGCAG- 3'). The primers used to amplify the *rickA* and *sca2* genes included homology arms that facilitated Gibson cloning (New England Biolabs, E2611S) into SspI-cut plasmids pET His6 MBP TEV LIC (Addgene #29656) or pET His6 GST TEV LIC (Addgene #29655) obtained from University of California, Berkeley, QB3 MacroLab.

To generate plasmids pET-MBP-NTDSca2, pET-MBP-ΔpolyPSca2, and pET-MBP-Sca2CTD to express Sca2 truncation derivatives, desired regions of the plasmid pET-MBP-Sca2 were amplified by PCR (primers: pET-MBP-NTDSca2: 5'-TGGATTAAAATTAGAAATATAAGATG-3' and 5'-TTTGCACTTGCTTCCCCCAC-3'; pET-MBP-ΔpolyPSca2, 5'-GTTGATCCTAAATCAGCAGC-3' and 5'-CATGAACTATATCTCCTTCTTAAAG-3'; pET-MBP-Sca2CTD, 5'-AATTATAAGTATATAATTTCGTATAGTACG-3' and 5'-CATGAACTATATCTCCTTCTTAAAG-3'). To generate plasmids pET-MBP-Sca2-L101A/K102A, pET-MBP-Sca2 was amplified with primers encoding the L101A/K102A mutations (primers: 5'-TTATGATACAGCGGCGAAAAATAGGAAAAATATAAAAAATAAAAAG-3' and 5'-GGATTAAATGTTGGACCTAATTC-3'). To generate pET-MBP-Sca2KCK, pET-MBP-Sca2 was amplified by PCR with primers encoding a C-terminal GGS linker and KCK motif (primers: 5'-AGCAAGTGCAAATGAATTGGAAGTGGATAAC-3' and 5'-TCCCCCACCGCTTCCACCGCCTTCATCACCACCAGTAATC-3'). The resulting PCR products where ligated using the KLD reaction mix (New England Biolabs, M0554S).

To generate plasmids pGEX-GST-Sca2-44 (aa 44-175) and pGEX-GST-Sca2-357 (and aa 357-464) for anti-Sca2 antibody production, gene sequences encoding the *R. bellii* Sca2 truncations were subcloned into pGEX-6P-3 (GE Healthcare, 28-9546-51).

Protein purification and fluorescent labeling

To express *R. bellii* GST-RickA and MBP-RickA, BL21-CodonPlus (DE3)-RIL *E. coli* (Agilent Technologies, 230245) were transformed with plasmid pET-GST-RickA or pET-MBP-RickA. For protein expression, bacteria were grown overnight at 37˚C in LB media. The overnight culture was then diluted 1:100 into 3 L of 2xYT media and grown to an OD_{600} of 0.5-0.8. Protein expression was induced by adding IPTG to 0.3 mM and bacteria were grown at 37˚C for an additional 2 h. Cells were pelleted at 4000 rpm for 20 min at 4˚C, resuspended in 30 mL either GST lysis buffer (50 mM Tris, pH 7.5, 250 mM KCl, 1 mM EDTA) or MBP lysis buffer (20 mM HEPES, pH 8, 200 mM NaCl, 1 mM EDTA) with 1 mg/mL lysozyme (Sigma, L4919) and protease inhibitors (10 µg/mL leupeptin, pepstatin, chymostatin (LPC) and 1 mM PMSF), and lysed by sonication (8-25 x 10s pulses, 30% amplitude). The lysate was centrifuged at 13,000 rpm in a Sorvall SS-34 rotor for 30 min at 4˚C. Lysate supernatant was run over Glutathione Sepharose 4B resin (GE Healthcare) or Amylose resin (New England Biolabs), washed with MBP or GST column buffer (the respective lysis buffer with 0.5 mM DTT), and eluted in GST column buffer with 10 mM glutathione or MBP column buffer with 10 mM maltose. MBP-RickA was used for antibody affinity purification as described below. GST-RickA was further purified by

gel filtration chromatography on a Superdex 200 Increase 10/300 GL column (Cytiva) equilibrated with Buffer A (20 mM HEPES, pH 7.5, 200 mM KCl, 2 mM EGTA, 2 mM EDTA, 0.5 mM DTT, 10% glycerol), then flash frozen in liquid N_2 and stored at -80˚C.

To express GST-Sca2-44 and GST-Sca2-357 for *R. bellii* Sca2 antibody generation, BL21-CodonPlus(DE3)-RIPL (Agilent Technologies, 230280) transformed with pGEX-GST-Sca2-44 or pGEX-GST-Sca2. Bacteria were grown overnight at 37˚C in 2xYT media, diluted 1:100 into 3 L of 2xYT media, and then grown again to an OD600 of 0.5-0.8. Protein expression was induced with 0.3-1 mM IPTG (Gold Biotechnology, 20-109) at 16˚C overnight. Cells were pelleted, resuspended in lysis buffer (50 mM Tris, 200 mM KCl, 1 mM EDTA, pH 7.5,) with 1 mg/mL lysozyme (Sigma) and protease inhibitors (10 µg/mL LPC and 1 mM PMSF), and lysed by sonication. Lysate was run over Glutathione Sepharose 4B (GE Healthcare) and washed with wash buffer (lysis buffer plus 0.5 mM DTT). PreScision Protease was added to the wash buffer for 16-18 h at 4˚C to cleave the GST tag, and cleaved protein was eluted with 1 column volume of wash buffer. Elutions were run over a Superdex 75 10/300 GL column (GE Healthcare) in 20 mM Tris, pH 7.5, 100 mM KCl, 1 mM EGTA, 2 mM EDTA, 0.5 mM DTT, 10% glycerol, then flash frozen and stored at -80˚C.

To express the *R. bellii* MPB-Sca2 proteins for use in actin assembly assays, BL21-CodonPlus (DE3)-RIPL *E. coli* cells (Agilent Technologies, 230280) transformed with expression plasmids pET-MBP-Sca2, pET-MBP-ΔpolyPSca2, pET-MBP-Sca2-L101A/K102A, pET-MBP-NTDSca2, or pET-MBP-Sca2CTD. Growth and expression conditions were as described above for expression at 16˚C. Cells were pelleted, lysed with lysis buffer (50 mM HEPES, pH 7.5, 500 mM KCl, 10 mM imidazole, 10 % glycerol) with 1 mg/mL lysozyme (Sigma) and protease inhibitors (GoldBio ProBlock Gold Bacterial Protease Inhibitor Cocktail, GB-108-2, Roche cOmplete EDTA-free Protease Inhibitor Cocktail, 4693159001, or APEX Protease Inhbitor Cocktail EDTA-free, K1007) followed by sonication (8-25 x 10s pulses, 30% amplitude). Lysate was run over an Ni-NTA resin (Qiagen), washed with column buffer (50 mM HEPES, pH 7.5, 500 mM KCl, 20 mM imidazole, 1 mM DTT, 10% glycerol), and eluted in elution buffer (50 mM HEPES, pH 7.5, 500 mM KCl, 250 mM imidazole, 1mM DTT, 10% glycerol). Elutions were run over a HiTrapQ HP column (Cytiva, 17-1153-01) with a 100 – 800 mM KCl gradient in anion exchange buffer (20 mM Tris, pH 7.5, 10% glycerol, 0.5 mM DTT) and then a Sephacryl S300 or Superdex 200 Increase 10/300 GL column (Cytiva) equilibrated with Buffer B (20 mM HEPES, pH 7.5, 500 mM KCl, 2 mM EGTA, 2 mM EDTA, 0.5 mM DTT, 10% glycerol). Anion exchange was not used when prepping the MBP-NTDSca2 protein. Proteins were flash frozen in liquid N_2 and stored at -80˚C.

To fluorescently label *R. bellii* Sca2 (Sca2-AF647), MBP-Sca2KCK was expressed as described for MBP-Sca2 proteins and purified as described for MBP-RickA. Post purification, the MBP-tag was cleaved with His-TEV protease for 1 h at room temperature and separated on a Superdex 200 Increase 10/300 GL column (Cytiva) equilibrated with Buffer A. Sca2KCK was dialyzed overnight into Buffer A with 1 mM TCEP (Sigma, 646547) instead of DTT. Equimolar amounts of Sca2KCK (35 µg) and AlexaFluor 647-maleimide (Invitrogen, A23047) were mixed and the maleimide reaction was allowed to proceed overnight at 4˚C. Excess dye was removed by dialysis into Buffer A before Sca2-AF647 was flash frozen in liquid N_2 and stored at -80˚C.

Antibody production, purification, and immunoblotting

To generate antiserum to *R. bellii* Sca2 (anti-RbSca2), Sca2-44-175 and Sca2-357-464 were expressed and purified as described above, mixed in equimolar amounts, and used to immunize two rabbits (Pocono Rabbit Farm & Laboratory, Inc). The generation of antiserum to *R. parkeri*

Sca2 (anti-RpSca2; (Haglund *et al.*, 2010)) and antiserum to *R. rickettsii* RickA (anti-RrRickA; (Jeng *et al.*, 2004)) were described previously. To affinity purify anti-RbSca2 or anti-RickA antibodies, 2.5 mg of *R. bellii* Sca2 truncations (equimolar amounts) or 500 µg of *R. bellii* MBP-RickA were conjugated to 1 ml of NHS-activated Sepharose 4 Fast Flow (GE Healthcare) in ligand-coupling buffer (200 mM $NaHCO_3$, pH 8.3, 500 mM NaCl) for 30 min at room temperature or overnight at 4˚C. Ligand-coupled resin was incubated with 10 ml of anti-RbSca2 serum or anti-RrRickA serum (*R. rickettsii* RickA is similar in sequence to *R. bellii* RickA). Serum was diluted in 10 ml binding buffer (20 mM Tris, pH 7.5) for 1 h at room temperature or overnight at 4˚C. Antibodies were eluted using 100 mM glycine, pH 2.5, and fractions were pooled and dialyzed overnight at 4˚C against PBS (137 mM NaCl, 2.7 mM KCl, 10 mM Na_2HPO_4, 1.8 mM KH_2PO_4, pH 7.4) for anti-RickA or TBS (150 mM NaCl, 50 mM Tris-Cl, pH 7.6) for anti-RbSca2. Antibodies were concentrated to 0.72 mg/mL (anti-RbRickA) and 2 mg/mL (anti-RbSca2) before flash freezing and storage at -80°C, or mixed with 50% glycerol and stored at -20°C.

For immunoblotting, $5x10^6$ of WT *R. bellii* from a 30% prep was diluted 1:1 with 2x Laemmli buffer (Bio-Rad, 1610737) and boiled for 10 min. The samples were run on a 10% SDS-PAGE gel and transferred to a PVDF membrane (Millipore, IPFL00010). The membrane was blocked in TBS-T (20 mM Tris, pH 8, 150 mM NaCl, 0.1% Tween 20) with 5% non-fat dry milk (Apex, 20-241) for 1 h. The membrane was then incubated with 1:1000 anti-RbSca2 or anti-RbRickA in TBS-T with 5% milk, washed 3x in TBS-T, and incubated for 1 h with 1:5000 mouse anti-rabbit HRP secondary antibody (Santa Cruz Biotechnology, sc-2357) in TBS-T with 5% milk, and washed again 3x with TBS-T. Following developing with the ECL HRP substrate kit (Advasta, K-12045-D20) for 45 s, bands were imaged on a ChemiDoc MB Imaging System (Bio-Rad).

Fixed cell imaging

For fixed-cell imaging of cells infected with *R. parkeri* or *R. bellii*, bacteria (WT, pRAM18dRGA, or pRAM18dR-2xCoTagBFP) from 30% prep frozen stocks were added to tissue culture media at an MOI of 0.6-10 (based on PFU measurements described above), aliquoted onto coverslips pre-seeded with 2×10^5 A549 or HMEC-1 cells, and centrifuged at 300 x g for 5 min at room temperature to facilitate infection. Infected cells were incubated at 33˚C for 1 h, washed 2x with PBS (Gibco, 10010072) to remove excess bacteria, and tissue culture media was replaced. Infections were allowed to proceed for 15 m - 24 h at 33˚C before cells were fixed with 4% paraformaldehyde (Ted Pella Inc, 18505) in PBS for 10 min at room temperature. For fixed-cell imaging of cells infected with *L. monocytogenes,* the cells were diluted into the relevant tissue culture media at an MOI of 5 (based on OD_{600} of 1.0 = $1x10^9$ CFU/ml *L. monocytogenes*; (Ghosh and Higgins, 2018)), and incubated at 37˚C for 15 min. A549 cells were infected as described above, and infections were allowed to proceed at for a total of 8 h before they were fixed as described above. For Arp2/3 inhibitor studies, coverslips were infected with *R. bellii* for 8 h and 24 h or *L. monocytogenes* for 8 h*,* as described above. At 1 h prior to fixation, coverslips were treated with 200 µM CK689 (Sigma, 182517), CK666 (Sigma, 182515), or CK869 (Sigma, C9124) dissolved in DMSO.

After fixation, coverslips were permeabilized with 0.5% Triton-X 100 (Sigma, T9284) in PBS (Gibco, 10010-023) for 5 min. For localization of surface RickA or Sca2, coverslips were blocked for 1 h with 2% BSA (Sigma, A4503) in PBS and then incubated with 1:1000 affinity purified anti-RbSca2, anti-RpSca2, or anti-RbRickA in PBS with 2% BSA for 1 h at room temperature. For localization of internal (total) RickA, after blocking, bacteria were permeabilized with lysozyme buffer (PBS, 50 mM glucose, 5 mM EDTA, 5 mg/ml lysozyme (Sigma), and 0.1% Triton X-100) in a humidified chamber for 20 min at 37˚C. For quantifying bacteria in Figure 4, coverslips were incubated with 1:500 rabbit anti-I7 (obtained from Ted Hackstadt at the NIH/NIAID Rocky

Mountain Laboratories) in PBS with 2% BSA for 30 min at room temperature. All coverslips were incubated with 1:500 568-phalloidin (Molecular Probes, A12380) and 1:500 anti-rabbit 488 (Invitrogen, A-11008) in PBS with 2% BSA for 30 min at room temperature. Coverslips were mounted in ProLong Gold Antifade (Invitrogen, P36930), allowed to cure overnight, and sealed with clear nail polish the next day.

Standard confocal imaging of bacteria, RickA, Sca2, and actin was carried out using a Nikon Ti Eclipse microscope equipped with a Yokogawa CSU-XI spinning disc confocal using the 100x VC (1.4 NA) Plan Apo objective and a Clara Interline CCD Camera (Andor Technology). Bacteria were used to localize regions of interest for imaging and 3.5-4.5 µm image stacks were taken with a step size of 0.15 µm to capture all actin tails present in the field of view. Images were imported into ImageJ2/Fiji (v2.9.0/1.53t) (Schindelin *et al.*, 2012) and Z Projection with max intensity was used to collapse the stack. Bacteria, actin tails, and RickA or Sca2 puncta were manually quantified and plotted in GraphPad Prism 10.3.1 (GraphPad Software, Inc.).

Lattice structured illumination microscopy images of Sca2 localization on *R. parkeri* and *R. bellii* were collected at the Rausser College of Natural Resources Biological Imaging Facility at the University of California, Berkeley, using a Zeiss Elyra 7 Lattice Structured Illumination Microscope system running Zen Black using the 63x/1.4NA objective and the system SCMOS cameras. Bacteria with actin tails were used to localize regions of interest for imaging 3-5.6 µm image stacks with a step size of 0.091 µm. Raw 3D images stacks were processed using the SIM function of Zen Black. SIM files were imported into Huygens Professional (Scientific Volume Imaging, v24.10) and image restoration (deconvolution) was performed using CMLE to 0.01% confidence.

To quantify and compare Sca2 localization and coverage of the *R. parkeri* versus *R. bellii* surface, deconvolved images stacks were analyzed using Imaris 10.2 (Oxford Instruments). Separate surfaces were created for bacteria and Sca2 to generate area (sum of triangle surfaces for Sca2), sphericity (surface area of a sphere with the same volume as the Sca2 surface/surface area of the Sca2 surface) and overlapped volume (volume of the overlap between the bacteria and Sca2 defined surfaces) values used for quantifying Sca2 coverage of *Rickettsia*. Results were plotted in GraphPad Prism 10.3.1 (Graphpad Software, Inc.). For actin tail intensity line scans, deconvolved images were imported into ImageJ2/Fiji (v2.9.0/1.53t) and a max intensity projection was made for the actin channel of each image. A 1.25 µm line segment was drawn perpendicular to the actin tail 0.5 µm from the base of the bacterium and the intensity values across the perpendicular line segment were saved for one actin tail per image. The intensity values were normalized to the smallest and largest value across individual actin tails and plotted in GraphPad Prism 10.3.1. The *R. parkeri* actin tail width was calculated from the distance between the two peak fluorescence values.

Live cell imaging

For live cell imaging, 1 x 10^6 A549 or HMEC-1 cells stably expressing RFP-F-tractin (generated as described above) were plated in a MatTek dish (MatTek, P35G-1.5-20-C) and incubated at 37˚C overnight. Mammalian cells were infected with *R. parkeri* pRAM18dRGA or *R. bellii* pRAM18dRGA at an MOI of 1, as described above. Immediately before imaging, media was changed to live cell imaging media (Live Cell Imaging Solution (Molecular Probes, A59688DJ), 10% FBS (ATLAS Biologics, FP-0500-A), 10 mM glucose (Fisher, D16), and 0.01% oxyrase (v/v) (Oxyrase Inc, OF-0005)). Dishes were imaged in an environmental chamber set to 33˚C on the Nikon Ti Eclipse microscope described above. Images were taken at 5 s intervals for 5 min in cells where actin tails were clearly observed.

Images were imported into ImageJ2/Fiji (v2.9.0/1.53t) (Schindelin *et al.*, 2012). To calculate motility speed, the Manual Tracking Plug-In was used to track individual bacteria with actin tails over the course of 1 m in 5 s intervals, with the total distance traveled in µm representing the speed µm/min. Motility efficiency was calculated by recording the X and Y pixel coordinates from t = 0 m and t = 1 m timepoints and then using the distance formula in Microsoft Excel to determine the straight-line distance in µm between the 0 m and 1 m coordinates. This value was divided by the total distance traveled over 1 m to obtain a motility efficiency value. Results were plotted in GraphPad Prism 10.3.1 (Graphpad Software, Inc.).

Bulk actin assembly assays

Rabbit skeletal muscle actin (Cytoskeleton, AKL99), pyrene labeled actin (Cytoskeleton, AP05), and rhodamine actin (Cytoskeleton, AR05) were dialyzed for 2-3 d in G-buffer (5 mM Tris, pH 7.5, 0.2 mM $CaCl_2$, 0.2 mM ATP, 0.5 mM DTT). The dialyzed actin was centrifuged at 100,000 x g in a TLA100 rotor (Beckman Coulter) using an Optima TLX Ultracentrifuge (Beckman Coulter) for 2 h at 4˚C. The top 3/4 of the supernatant was collected and run over a Superdex 200 Increase 10/300 GL column (Cytiva) equilibrated with G-buffer. The fractions corresponding to the latter half of the actin peak (the smaller Stokes radius) were combined and used. Purified Arp2/3 complex (Cytoskeleton, RP01P) was resuspended in milliQ water according to the manufacturer instructions.

Pyrene actin assembly assays were performed by combining 1 µM G-actin mix (10% pyrene labeled) with purified proteins, Buffer A, 10x initiation buffer (10 mM $MgCl_2$, 10 mM EGTA, 5 mM ATP, 500 mM KCl) with a final KCl concentration of 96 mM. Fluorescence was measured in two replicates per reaction condition, in three independent experiments, using a Tecan Infinite F200 Pro plate reader and Magellan software v7.1 at 20 s intervals with a 365 nm excitation and 405 nm emission filters. Each curve was baseline-corrected using an average of the first 3 values and graphed in Prism 10.3.1 (GraphPad Software, Inc).

For $t_{1/2\ max}$ calculations, the raw fluorescence values from the two replicates for each sample condition were averaged and normalized to the smallest and largest values using Prism 10.3.1. $t_{1/2\ max}$ calculations were performed with the normalized values as previously outlined (Doolittle et al., 2013) in Microsoft Excel. *R. bellii* Sca2 $t_{1/2\ max}$ values were normalized to the $t_{1/2\ max}$ value for actin alone for 3 separate experiments and plotted in Prism 10.3.1 (GraphPad Software, Inc).

TIRF imaging of actin filaments

To make NEM-myosin for immobilizing actin filaments, myosin (Cytoskeleton Inc., MY02) was resuspended in 10 mM imidazole, pH 7 and 0.5 M KCl. NEM (Sigma, E3876) was added at >10-fold molar excess to myosin and allowed to react at room temperature for 1 h before dialyzing overnight at 4˚C into 2x HS-TBS (100 mM Tris-HCl, pH 7.5, 1.2 M KCl). Glycerol was added to 50%, sodium azide to 0.02%, and aliquots were stored at -20˚C. Actin for TIRF studies was prepared as described above.

Flow cells were prepared using 22x22 mm n=1.5 coverslips (VWR, 48366-227), which were washed for 15 min 0.02% Hellmanex III (Hellma Analytics), 3x with MilliQ water, 15 min in 0.5 M NaOH, 3x with MilliQ water, then dried with a light stream of air. Double-sided Scotch tape was placed on ethanol cleaned microscope slides to create 2 chambers. Cleaned coverslips were placed on top of the tape and pressed with a pipette tip to seal. A solution of 10 nM NEM-myosin in HS-TBS (50 mM Tris-HCl, pH 7.5, 600 mM NaCl) was flowed into chambers for 1 m, then chambers were washed twice with HS-BSA (50 mM Tris-HCl, pH 7.5, 600 mM NaCl, 1%

BSA), twice with 2x LS-BSA (50 mM Tris-HCl, pH 7.5, 150 mM NaCl, 1% BSA), and once with 1x TIRF buffer (10 mM imidazole, pH 7, 50 mM KCl, 1 mM $MgCl_2$, 1 mM EGTA, 50 mM DTT, 0.2 mM ATP, 50 mM $CaCl_2$, 15 mM glucose, 20 µg/mL catalase, 100 µg/mL glucose oxidase, 0.4% methylcellulose).

For TIRF reactions, a solution of 2 µM actin monomers (33% rhodamine-labeled) was supplemented with $MgCl_2$ to 50 µM and EDTA to 0.2 mM for 5 min to exchange Ca^{2+} for Mg^{2+}. When relevant, 0.5 or 5 nM Sca2-AF647 and 3 µM profilin (purified as previously described (Fedorov *et al.*, 1994)), or an equivalent volume of Buffer A was added. 5 min before imaging, 2x TIRF buffer was added at a 1:1 ratio to the actin and proteins of interest and the mix was flowed into the flow cell.

Imaging was carried out on a Nikon Ti Eclipse Ti2 inverted microscope equipped with a Nikon 60x/1.49 NA CFI Apo TIRF objective and temperature chamber set to 25˚C (Oko labs). Single-plane TIRF images were illuminated with a LUNF 4-line laser launch and iLas2 TIRF/FRAP module (Gataca Systems) and captured with an Orca Fusion Gen III sCMOS camera (Hamamatsu) every 5 s for 15-20 m with NIS Elements software (Nikon). For each reaction, the growth of 5 actin filaments in 3 separate movies were measured. Elongation rate was determined over the course of 300 s by manually tracing the barbed ends (fast growing end with visually stable attachment point) of each filament 60 frames apart in ImageJ2/Fiji (v2.9.0/1.53t) and graphed in Prism 10.3.1 (GraphPad Software, Inc).

Protein alignments, motif identification, and structure prediction

Protein alignments and trees were generated using Geneious Prime 2025.0.3 (https://www.geneious.com). *Rickettsia* RickA sequences were aligned using the Geneious global alignment MUSCLE alignment algorithms. Post alignment, isolated amino acids in RickA were shifted to group with the most relevant neighboring cluster of amino acids. *R. parkeri* strain Portsmouth and *R. bellii* strain RML 369-C RickA and Sca2 sequences were submitted to InterPro for sequence motif analysis (Blum *et al.*, 2024). Protein sequences were submitted to the AlphaFold 3 server for structure prediction (Abramson *et al.*, 2024).

Acknowledgements

We thank Erin Goley for providing the pRAM18dR-2xCoTagBFP plasmid for using in making fluorescent *R. bellii* and *R. parkeri*. Thank you to Chris Jeans at the UC Berkeley QB3 MacroLab and Joanna Idrovo for helping with protein expression and purification of MBP-Sca2 proteins. We also thank Denise Schichnes at the UC Berkeley RCNR Biological Imaging Facility, Samantha Smith, and Lucy Brennan for technical advice and training about microscopy and about protein purification.

Figures

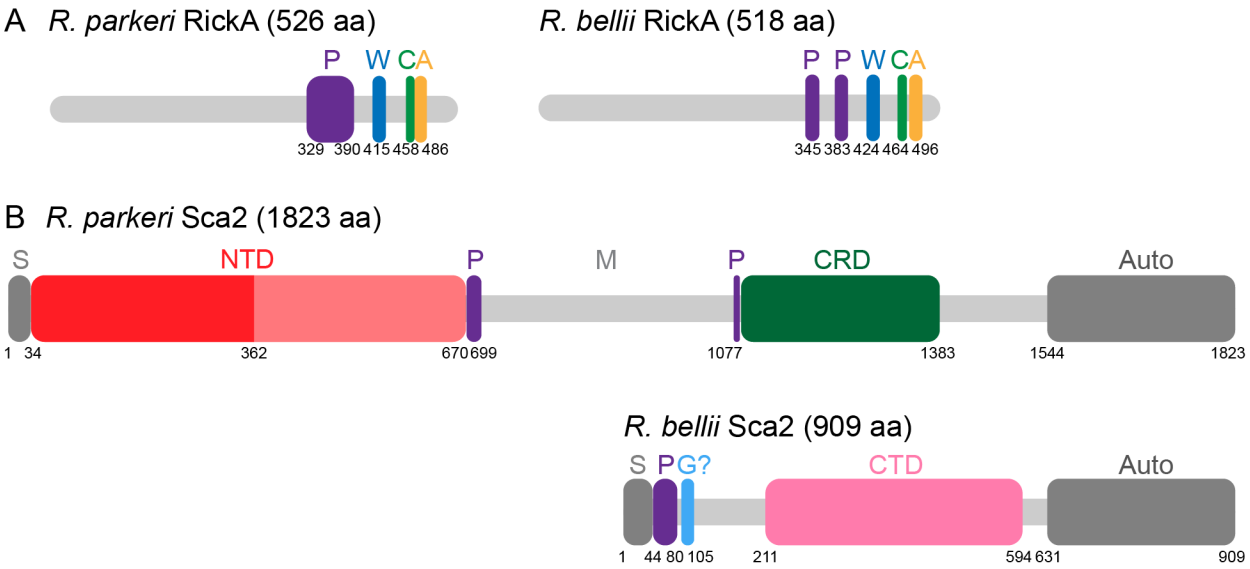

FIGURE 1. RickA domain organization is conserved, whereas Sca2 domain organization is more variable. (A) RickA from *R. parkeri* and *R. bellii* share a common domain architecture. (B) Sca2 proteins from *R. parkeri* and *R. bellii* differ considerably in their domain architecture. Abbreviations in (A) and (B): P = poly-proline or proline-rich domain, W = WASP homology-2 (WH2) motif, C = central motif, A = acidic motif, S = signal sequence, NTD = N-terminal domain (the darker half denotes the location of helical N-terminal repeats), M = middle domain, G? = putative G-actin binding domain, CRD = C-terminal repeat domain, CTD = C-terminal domain, Auto = autotransporter domain.

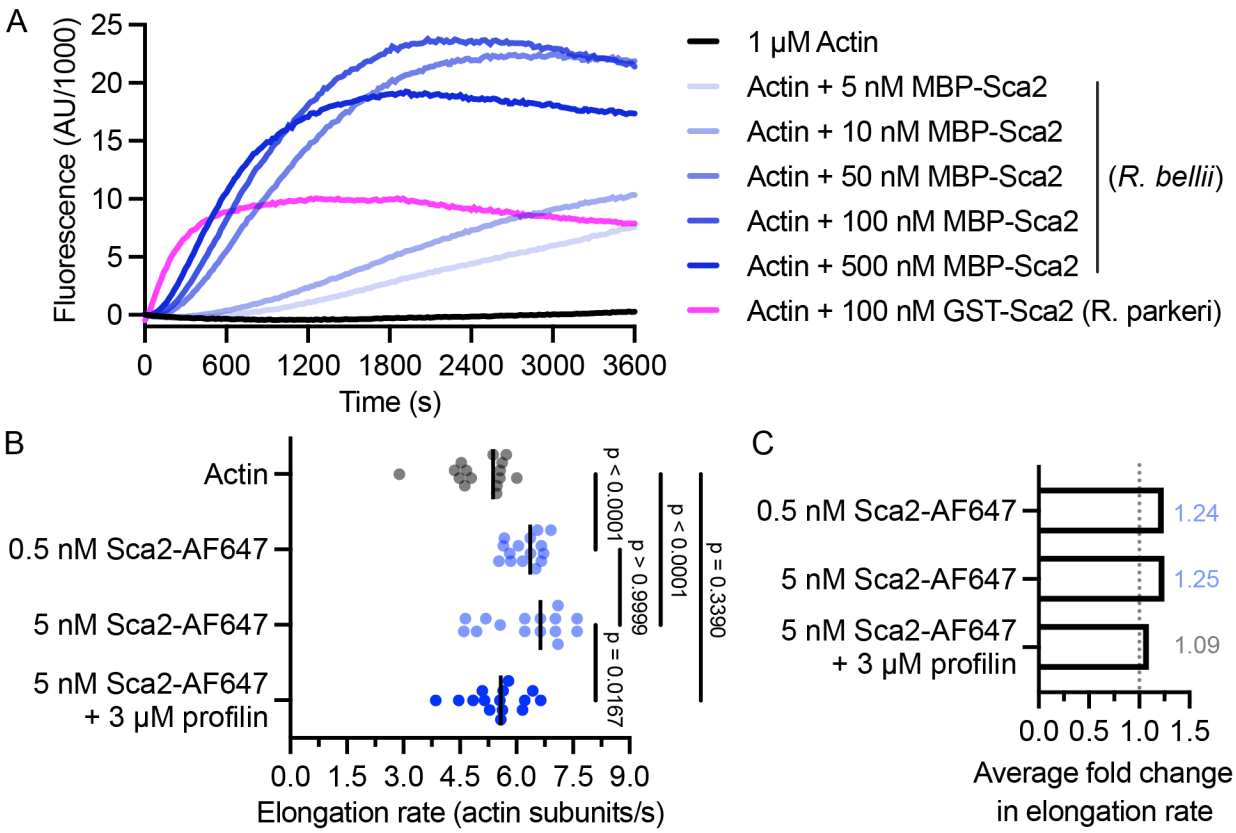

FIGURE 2. Sca2 from *R. bellii* nucleates actin filaments and promotes filament elongation. (A) Kinetics of assembly of 1 μM actin (10% pyrene-labeled) with the indicated concentrations of the *R. bellii* MBP-Sca2 or *R. parkeri* GST-Sca2 passenger domains. (B) Quantification of actin filament barbed-end elongation rates in TIRF assays performed with 1 μM actin (33% rhodamine-labeled) without or with the indicated concentrations of *R. bellii* Sca2-AF647 and 3 μM profilin. Vertical black lines indicate median elongation rate. N = 3 independent experiments per treatment, n = 5 filaments per experiment. Significance was determined using a one-way ANOVA with a Tukey's multiple comparison post-test. (D) Average fold change in barbed end actin filament elongation rates for the indicated concentrations of Sca2-AF647 and profilin relative to actin alone (grey dotted line).

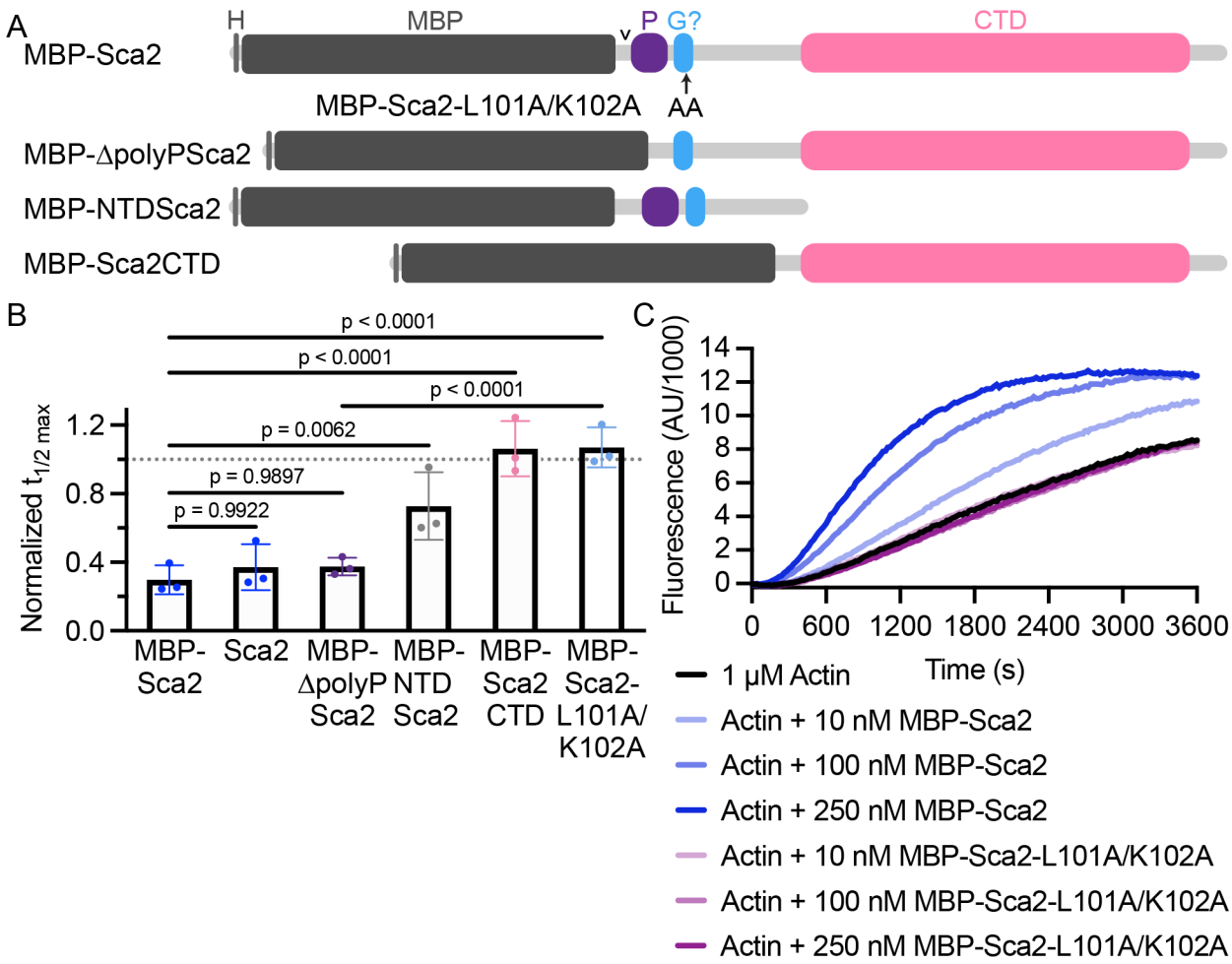

FIGURE 3. The *R. bellii* Sca2 N-terminus (aa 43-210), including a putative G-actin binding domain, is necessary to promote actin nucleation. (A) Diagram of truncated and mutated derivatives of *R. bellii* Sca2. H = 6x-His tag, MBP = Maltose binding protein tag, P = poly-proline domain, G? = G-actin binding domain, CTD = C-terminal domain, arrowhead = TEV protease cleavage site. The MBP-Sca2-L101A/K102A protein contains two point mutations in the G-actin binding domain. (B) Calculated $t_{1/2\ max}$ from pyrene-actin polymerization assays, normalized to actin alone (grey dotted line), for the indicated *R. bellii* Sca2 variants at 70 nM with average values noted in the bars. N = 3 experiments for each protein, n = 2 replicates per experiment. Error bars indicate SD. Significance was determined using a one-way ANOVA with a Tukey's multiple comparisons test. (C) Kinetics of assembly of 1 μM actin (10% pyrene-labeled) with the indicated concentrations of the *R. bellii* MBP-Sca2 or MBP-Sca2-L101A/K102A.

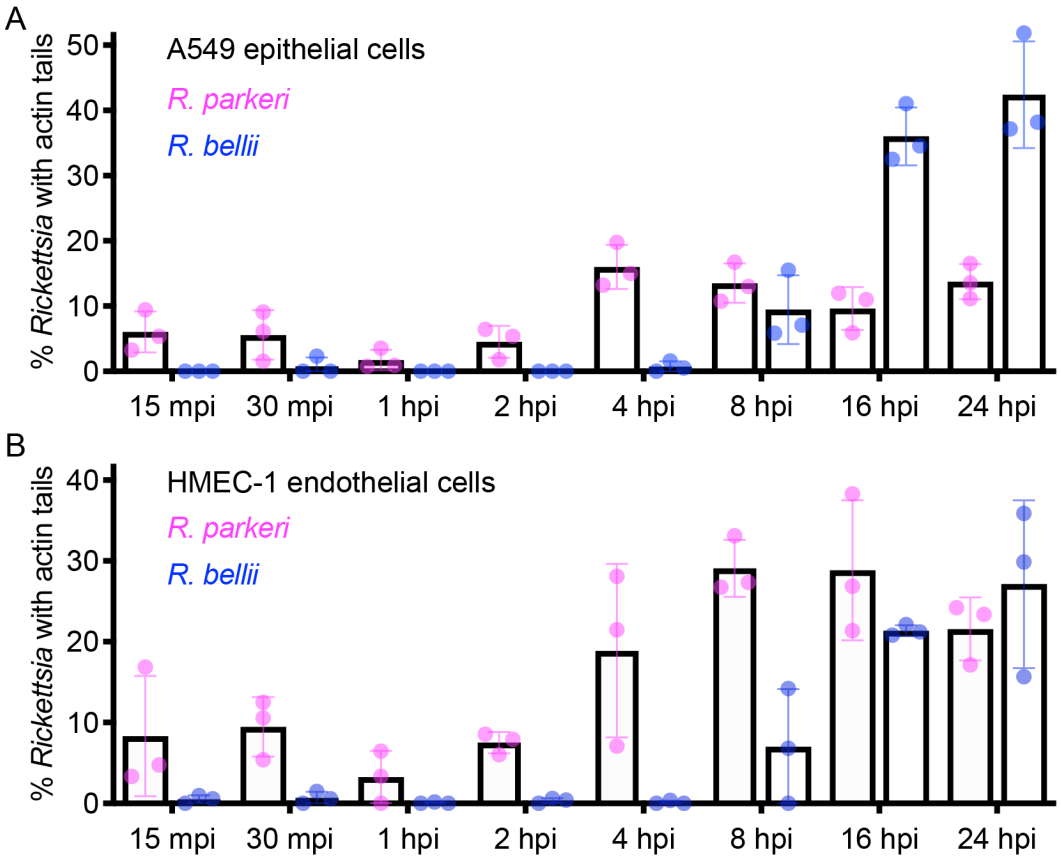

FIGURE 4. *R. bellii* has a single phase of actin-based motility. Quantification of *R. parkeri* (magenta) and *R. bellii* (blue) actin tails in infected (A) A549 human epithelial cells and (B) HMEC-1 human endothelial cells from 15 mpi to 24 h hpi. Error bars indicate SD. N = 3 independent experiments, n ≥ 51 bacteria per experiment per time point.

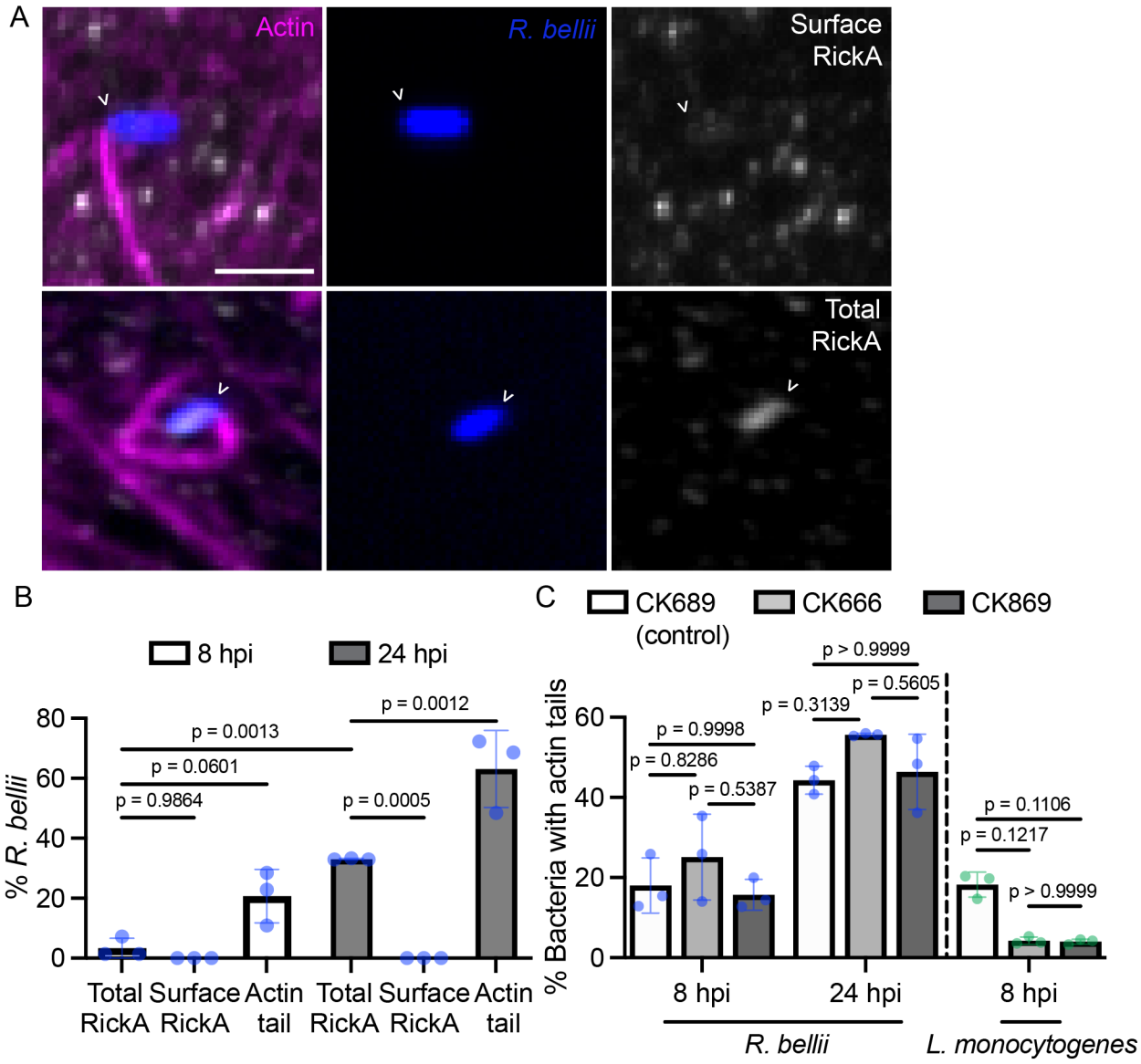

FIGURE 5. RickA was not observed on the *R. bellii* surface and Arp2/3 complex inhibition did not impact *R. bellii* motility. (A) Representative maximum-projection images of *R. bellii* (blue) in infected A549 cells immuno-stained for surface-localized and total RickA (white) and actin filaments (magenta) at 24 hpi. The bacterial pole associated with an actin tail is indicated with open arrowheads. Scale bar = 1 μm. (B) Percentage of *R. bellii* with total and surface-localized RickA at 8 and 24 hpi. N = 3 independent experiments, n ≥ 95 bacteria per experiment per time point. Significance was determined using a two-way ANOVA with a Tukey's multiple comparisons post-test. (C) Percentage of *L. monocytogenes* and *R. bellii* with actin tails at 8 and/or 24 hpi in the presence of Arp2/3 complex-inhibitors CK666 or CK869, or inactive control compound CK689. N = 3 independent experiments, n ≥ 139 bacteria per experiment per time point. Error bars indicate SD. Significance was determined using a one-way ANOVA with a Tukey's multiple comparisons post-test.

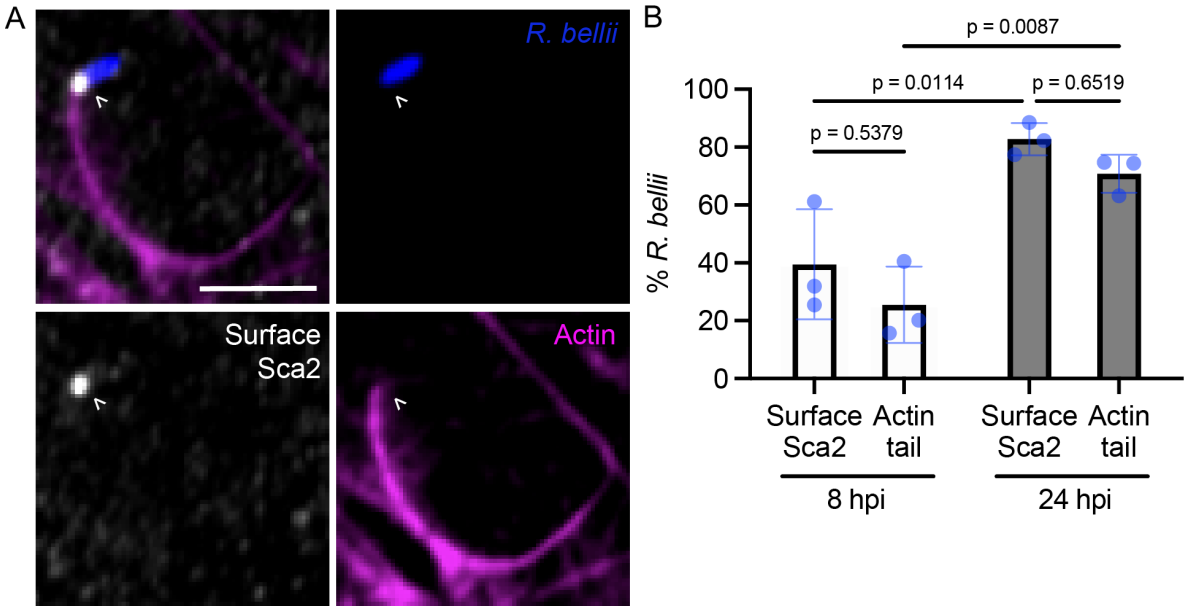

FIGURE 6. Sca2 localizes to the surface of *R. bellii* in correlation with the formation of actin tails. (A) Representative confocal maximum-intensity projection image of *R. bellii* (blue) with actin filaments (magenta) and Sca2 (white) in infected A549 cells at 8 hpi. The bacterial pole associated with an actin tail is indicated with open arrowheads. Scale bar = 2 µm. (B) Percentage of *R. bellii* with polar Sca2 and frequency of actin tails. N = 3 independent experiments, n ≥ 94 bacteria per experiment per time point. Error bars indicate SD. Significance was determined using a two-way ANOVA with a Tukey's multiple comparisons post-test.

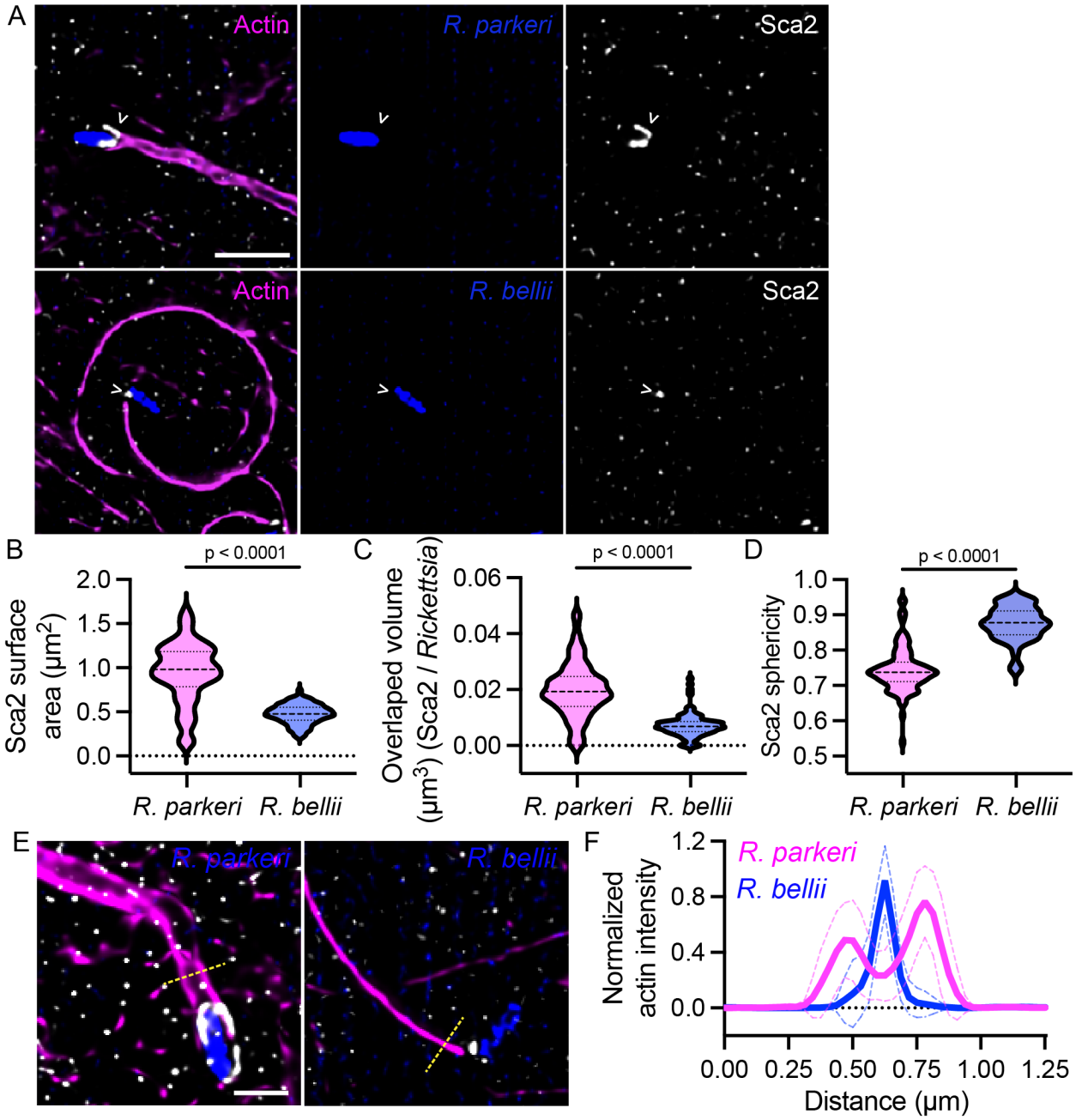

FIGURE 7. Sca2 morphology and actin tail organization differs between *R. bellii* and *R. parkeri*. (C) Deconvolved lattice structured illumination (LSIM) maximum projections of A549s infected for 24 h with *R. parkeri* (blue) or *R. bellii* (blue) stained actin filaments (magenta) and Sca2 (white). Scale bars = 2 μm. Quantification of *R. parkeri* and *R. bellii* Sca2 (D) surface area and (E) sphericity, and (F) overlapped volume. Error bars indicate SD. N = 3 independent replicates, n ≥ 229 bacteria per species per replicate. Significance was determined using a Welch's t-test. (E) Maximum projections of deconvolved LSIM micrographs showing representative actin tail (magenta) intensity traces (dashed yellow line) positioned 0.5 μm from the start of the actin tail at the pole of the bacterium (blue) with Sca2 (white) in infected A549 cells. Scale bar = 1 μm. (F) Plot of cumulative *R. parkeri* and *R. bellii* actin tail intensity traces. N = 3 independent experiments, n = 18 traces per *Rickettsia* species.

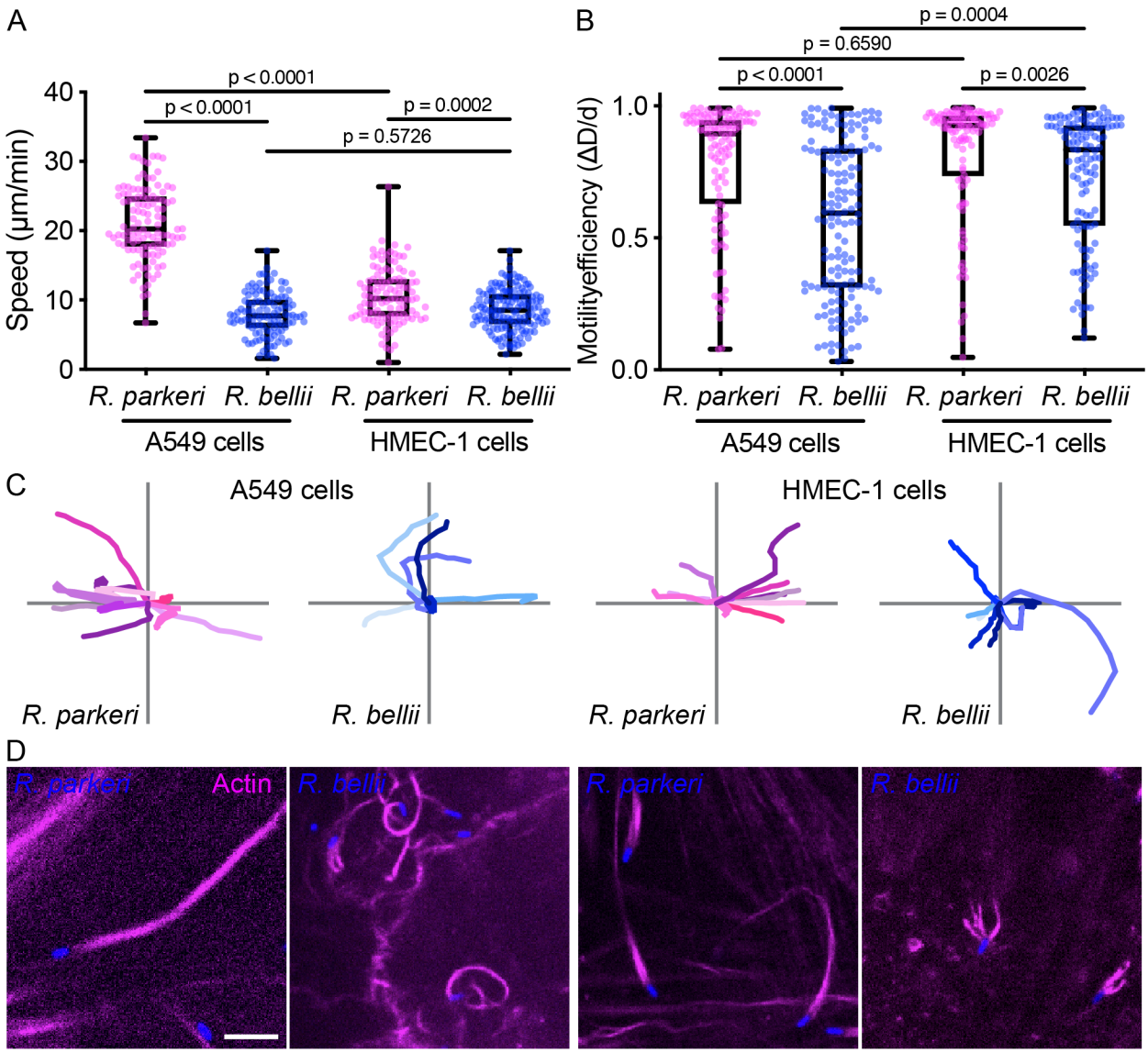

FIGURE 8. Actin-based motility parameters and actin tail organization differ between *R. bellii* and *R. parkeri* as well as host cell lines. (A) Speed of *R. parkeri* and *R. bellii* at 24 hpi in A549 and HMEC-1 cell lines. (B) Motility efficiency (ΔD/d) of *R. parkeri* and *R. bellii* at 24 hpi in A549 and HMEC-1 in 1 min intervals. N = 3 - 5 independent experiments per *Rickettsia* species and host cell line, n ≥ 110 bacteria per *Rickettsia* species and host cell line. Significance was determined using a one-way ANOVA with a (A) Tukey's multiple comparisons or (B) Kruskal-Wallis post-test. (C) Motility traces of 10 representative *R. parkeri* (magenta) and *R. bellii* (blue) in infected A549 or HMEC-1 cell lines. Some traces are not clearly visible due to overlapping tracks. (D) Representative still images of *R. parkeri* and *R. bellii* (blue) with actin tails (magenta), showing differences in actin organization. Scale bar = 5 µm.

References

Abramson, J, Adler, J, Dunger, J, Evans, R, Green, T, Pritzel, A, Ronneberger, O, Willmore, L, Ballard, AJ, Bambrick, J, *et al.* (2024). Accurate structure prediction of biomolecular interactions with AlphaFold 3. *Nature* 630, 493–500.

Alqassim, SS (2022). Functional Mimicry of Eukaryotic Actin Assembly by Pathogen Effector Proteins. *Int J Mol Sci* 23, 11606.

Alqassim, SS, Lee, I-G, and Dominguez, R (2019). *Rickettsia* Sca2 Recruits Two Actin Subunits for Nucleation but Lacks WH2 Domains. *Biophys J* 116, 540–550.

Blanc, G, Ngwamidiba, M, Ogata, H, Fournier, P-E, Claverie, J-M, and Raoult, D (2005). Molecular Evolution of *Rickettsia* Surface Antigens: Evidence of Positive Selection. *Mol Biol Evol* 22, 2073–2083.

Blanc, G, Ogata, H, Robert, C, Audic, S, Suhre, K, Vestris, G, Claverie, J-M, and Raoult, D (2007). Reductive Genome Evolution from the Mother of *Rickettsia*. *PLoS Genet* 3, e14.

Blum, M, Andreeva, A, Florentino, LC, Chuguransky, SR, Grego, T, Hobbs, E, Pinto, BL, Orr, A, Paysan-Lafosse, T, Ponamareva, I, *et al.* (2024). InterPro: the protein sequence classification resource in 2025. *Nucleic Acids Res* 53, D444–D456.

Breitsprecher, D, and Goode, BL (2013). Formins at a glance. *J Cell Sci* 126, 1–7.

Burke, TP, Engström, P, Tran, CJ, Langohr, IM, Glasner, DR, Espinosa, DA, Harris, E, and Welch, MD (2021). Interferon receptor-deficient mice are susceptible to eschar-associated rickettsiosis. eLife 10, e67029.

Burkhardt, NY, Baldridge, GD, Williamson, PC, Billingsley, PM, Heu, CC, Felsheim, RF, Kurtti, TJ, and Munderloh, UG (2011). Development of Shuttle Vectors for Transformation of Diverse *Rickettsia* Species. *PLoS ONE* 6, e29511.

Cao, L, Huang, S, Basant, A, Mladenov, M, and Way, M (2024). CK-666 and CK-869 differentially inhibit Arp2/3 iso-complexes. *EMBO Rep* 25, 3221–3239.

Carman, PJ, Rebowski, G, Dominguez, R, and Alqassim, SS (2023). Single particle cryo-EM analysis of *Rickettsia conorii* Sca2 reveals a formin-like core. *J Struct Biol* 215, 107960.

Colonne, PM, Winchell, CG, and Voth, DE (2016). Hijacking Host Cell Highways: Manipulation of the Host Actin Cytoskeleton by Obligate Intracellular Bacterial Pathogens. *Front Cell Infect Microbiol* 6, 107.

Dominguez, R (2016). The WH2 Domain and Actin Nucleation: Necessary but Insufficient. *Trends Biochem Sci* 41, 478–490.

Ducka, AM, Joel, P, Popowicz, GM, Trybus, KM, Schleicher, M, Noegel, AA, Huber, R, Holak, TA, and Sitar, T (2010). Structures of actin-bound Wiskott-Aldrich syndrome protein homology 2 (WH2) domains of Spire and the implication for filament nucleation. *Proc Natl Acad Sci* 107, 11757–11762.

Faix, J, and Rottner, K (2022). Ena/VASP proteins in cell edge protrusion, migration and adhesion. *J Cell Sci* 135.

Fan, E, Chauhan, N, Udatha, DBRKG, Leo, JC, and Linke, D (2016). Type V Secretion Systems in Bacteria. *Microbiol Spectr* 4, 10.1128/microbiolspec.vmbf-0009–2015.

Fedorov, AA, Pollard, TD, and Almo, SC (1994). Purification, Characterization and Crystallization of Human Platelet Profilin Expressed in *Escherichia coli*. *J Mol Biol* 241, 480–482.

Figueroa-Cuilan, WM, Irazoki, O, Feeley, M, Smith, E, Nguyen, T, Cava, F, and Goley, ED (2023). Quantitative analysis of morphogenesis and growth dynamics in an obligate intracellular bacterium. *Mol Biol Cell* 34, ar69.

Gautreau, AM, Fregoso, FE, Simanov, G, and Dominguez, R (2022). Nucleation, stabilization, and disassembly of branched actin networks. *Trends Cell Biol* 32, 421–432.

Ghosh, P, and Higgins, DE (2018). *Listeria monocytogenes* Infection of the Brain. *J Vis Exp*.

Gillespie, JJ, Kaur, SJ, Rahman, MS, Rennoll-Bankert, K, Sears, KT, Beier-Sexton, M, and Azad, AF (2015). Secretome of obligate intracellular *Rickettsia*. *FEMS Microbiol Rev* 39, 47–80.

Gouin, E, Egile, C, Dehoux, P, Villiers, V, Adams, J, Gertler, F, Li, R, and Cossart, P (2004). The RickA protein of *Rickettsia conorii* activates the Arp2/3 complex. *Nature* 427, 457–461.

Gouin, E, Gantelet, H, Egile, C, Lasa, I, Ohayon, H, Villiers, V, Gounon, P, Sansonetti, PJ, and Cossart, P (1999). A comparative study of the actin-based motilities of the pathogenic bacteria *Listeria monocytogenes, Shigella flexneri* and *Rickettsia conorii*. *J Cell Sci* 112, 1697–1708.

Gouin, E, Welch, MD, and Cossart, P (2005). Actin-based motility of intracellular pathogens. *Curr Opin Microbiol* 8, 35–45.

Guillotte, ML, Chandler, CE, Verhoeve, VI, Gillespie, JJ, Driscoll, TP, Rahman, MS, Ernst, RK, and Azad, AF (2021). Lipid A Structural Divergence in *Rickettsia* Pathogens. *mSphere* 6, 10.1128/msphere.00184-21.

Haglund, CM, Choe, JE, Skau, CT, Kovar, DR, and Welch, MD (2010). *Rickettsia* Sca2 is a bacterial formin-like mediator of actin-based motility. *Nat Cell Biol* 12, 1057–1063.

Harris, EK, Jirakanwisal, K, Verhoeve, VI, Fongsaran, C, Suwanbongkot, C, Welch, MD, and Macaluso, KR (2018). Role of Sca2 and RickA in the Dissemination of *Rickettsia* parkeri in *Amblyomma maculatum*. *Infect Immun* 86, 10.1128/iai.00123-18.

Heinzen, RA, Hayes, SF, Peacock, MG, and Hackstadt, T (1993). Directional actin polymerization associated with spotted fever group *Rickettsia* infection of Vero cells. *Infect Immun* 61, 1926–1935.

Jeng, RL, Goley, ED, D'Alessio, JA, Chaga, OY, Svitkina, TM, Borisy, GG, Heinzen, RA, and Welch, MD (2004). A *Rickettsia* WASP-like protein activates the Arp2/3 complex and mediates actin-based motility. *Cell Microbiol* 6, 761–769.

Johnson, HW, and Schell, MJ (2009). Neuronal IP3 3-Kinase is an F-actin–bundling Protein: Role in Dendritic Targeting and Regulation of Spine Morphology. *Mol Biol Cell* 20, 5166–5180.

Karkouri, KE, Ghigo, E, Raoult, D, and Fournier, P-E (2022). Genomic evolution and adaptation of arthropod-associated *Rickettsia*. *Sci Rep* 12, 3807.

Kleba, B, Clark, TR, Lutter, EI, Ellison, DW, and Hackstadt, T (2010). Disruption of the *Rickettsia rickettsii* Sca2 Autotransporter Inhibits Actin-Based Motility. *Infect Immun* 78, 2240–2247.

Lamason, RL, Bastounis, E, Kafai, NM, Serrano, R, Álamo, JC del, Theriot, JA, and Welch, MD (2016). *Rickettsia* Sca4 Reduces Vinculin-Mediated Intercellular Tension to Promote Spread. *Cell* 167, 670-683.e10.

Lamason, RL, and Welch, MD (2017). Actin-based motility and cell-to-cell spread of bacterial pathogens. *Curr Opin Microbiol* 35, 48–57.

Lehman, SS, Verhoeve, VI, Driscoll, TP, Beckmann, JF, and Gillespie, JJ (2024). Metagenome diversity illuminates the origins of pathogen effectors. *mBio* 15, e00759-23.

Madasu, Y, Suarez, C, Kast, DJ, Kovar, DR, and Dominguez, R (2013). *Rickettsia* Sca2 has evolved formin-like activity through a different molecular mechanism. *Proc Natl Acad Sci* 110, E2677–E2686.

Narra, HP, Sahni, A, Alsing, J, Schroeder, CLC, Golovko, G, Nia, AM, Fofanov, Y, Khanipov, K, and Sahni, SK (2020). Comparative transcriptomic analysis of *Rickettsia conorii* during in vitro infection of human and tick host cells. *BMC Genom* 21, 665.

Nolen, BJ, Tomasevic, N, Russell, A, Pierce, DW, Jia, Z, McCormick, CD, Hartman, J, Sakowicz, R, and Pollard, TD (2009). Characterization of two classes of small molecule inhibitors of Arp2/3 complex. *Nature* 460, 1031–1034.

Pan, Y-S, Cui, X-M, Du, L-F, Xia, L-Y, Du, C-H, Bell-Sakyi, L, Zhang, M-Z, Zhu, D-Y, Dong, Y, Wei, W, *et al.* (2022). Coinfection of Two Rickettsia Species in a Single Tick Species Provides New Insight into *Rickettsia-Rickettsia* and *Rickettsia*-Vector Interactions. *Microbiol Spectr* 10, e02323-22.

Reed, SCO, Lamason, RL, Risca, VI, Abernathy, E, and Welch, MD (2014). *Rickettsia* Actin-Based Motility Occurs in Distinct Phases Mediated by Different Actin Nucleators. *Curr Biol* 24, 98–103.

Rymaszewska, A, and Piotrowski, M (2024). *Rickettsia* Species: Genetic Variability, Vectors, and Rickettsiosis—A Review. *Pathogens* 13, 661.

Schindelin, J, Arganda-Carreras, I, Frise, E, Kaynig, V, Longair, M, Pietzsch, T, Preibisch, S, Rueden, C, Saalfeld, S, Schmid, B, *et al.* (2012). Fiji: an open-source platform for biological-image analysis. *Nat Methods* 9, 676–682.

Scott, AT, Vondrak, CJ, Sanderlin, AG, and Lamason, RL (2022). Rickettsia parkeri. *Trends Microbiol* 30, 511–512.

Serio, AW, Jeng, RL, Haglund, CM, Reed, SC, and Welch, MD (2010). Defining a Core Set of Actin Cytoskeletal Proteins Critical for Actin-Based Motility of *Rickettsia*. *Cell Host Microbe* 7, 388–398.

Shaner, NC, Lin, MZ, McKeown, MR, Steinbach, PA, Hazelwood, KL, Davidson, MW, and Tsien, RY (2008). Improving the photostability of bright monomeric orange and red fluorescent proteins. *Nat Methods* 5, 545–551.

Shere, KD, Sallustio, S, Manessis, A, D'Aversa, TG, and Goldberg, MB (1997). Disruption of IcsP, the major *Shigella* protease that cleaves IcsA, accelerates actin-based motility. *Mol Microbiol* 25, 451–462.

Steinhauer, J, Agha, R, Pham, T, Varga, AW, and Goldberg, MB (1999). The unipolar *Shigella* surface protein IcsA is targeted directly to the bacterial old pole: IcsP cleavage of IcsA occurs over the entire bacterial surface. *Mol Microbiol* 32, 367–377.

Stradal, TEB, and Schelhaas, M (2018). Actin dynamics in host–pathogen interaction. *FEBS Lett* 592, 3658–3669.

Teysseire, N, Chiche-Portiche, C, and Raoult, D (1992). Intracellular movements of *Rickettsia conorii* and *R. typhi* based on actin polymerization. *Res Microbiol* 143, 821–829.

Tran, CJ, Zubair-Nizami, Z, Langohr, IM, and Welch, MD (2025). The *Rickettsia* actin-based motility effectors RickA and Sca2 contribute differently to cell-to-cell spread and pathogenicity. *mBio* 16, e02563-24.

Valencia, DA, and Quinlan, ME (2021). Formins. *Curr Biol* 31, R517–R522.

Van Kirk, LS, Hayes, SF, and Heinzen, RA (2000). Ultrastructure of *Rickettsia rickettsii* Actin Tails and Localization of Cytoskeletal Proteins. *Infect Immun* 68, 4706–4713.

Vizcarra, CL, and Quinlan, ME (2017). Actin filament assembly by bacterial factors VopL/F: Which end is up? *J Cell Biol* 216, 1211–1213.

Welch, MD, Iwamatsu, A, and Mitchison, TJ (1997). Actin polymerization is induced by Arp 2/3 protein complex at the surface of *Listeria monocytogenes*. *Nature* 385, 265–269.